An Efficient Image Reconstruction Method for Low−Dose Computed Tomography

Thesis submitted in partial fulfillment of the requirements for the award of degree of

Master of Engineering

in

Computer Science and Engineering

Submitted by

Kavkirat Kaur

(Roll no: 801632021)

Under the supervision of

Dr. Shailendra Tiwari
Assistant Professor, CSED

THAPAR INSTITUTE
OF ENGINEERING & TECHNOLOGY
(Deemed to be University)

COMPUTER SCIENCE AND ENGINEERING DEPARTMENT
THAPAR INSTITUTE OF ENGINEERING AND TECHNOLOGY
PATIALA-147004

June 2018

Certificate

I hereby certify that the work, which is being presented in the thesis, entitled "*An Efficient Image Reconstruction Method for Low–Dose Computed Tomography*", in partial fulfillment of the requirements for the award of the degree of Master of Engineering in *Computer Science and Engineering* and submitted in Computer Science Department of Thapar Institute of Engineering and Technology (Deemed to be University), Patiala is an authentic record of my own work carried out under the supervision of *Dr. Shailendra Tiwari* and refers other researcher's work which are duly listed in the reference section.

The matter presented in this thesis has not been submitted elsewhere for the award of any other degree of this or any other University.

Kavkirat Kaur
Signature

Kavkirat Kaur

This is to certify that the above statement made by the candidate is correct and true to the best of my knowledge.

Dr. Shailendra Tiwari
Assistant Professor,
CSED

Abstract

The Computed Tomography (CT) has made a tremendous growth in medical imaging field for for the different applications like: clinical diagnosis, detection, and interventions over the past few decades. Recent researches in medical science have significantly improvised the perception of scientist and Physician's to better understand the cause of the disease that affects the human system and how the treatment process works behind it. However, excessive use of X-ray radiation may have some harmful effects such as genetic disorder, cancer syndrome and other harmful diseases. So, minimizing the radiations from CT has been a major concern. Therefore, low-dose CT is gaining the interest of researchers. There are many methods proposed over the past few decades, still many problems are faced.

In this work, we have presented two new statistical image reconstruction algorithm by proposing a suitable regularisation method. The proposed framework is the combination of two basic terms namely data fidelity and regularisation. Maximising the log likelihood gives the data fidelity term, which represents the distribution of noise in low-dose CT images. Maximum likelihood expectation maximization algorithm (MLEM) is introduced as a data-fidelity term in both the frameworks.

In the former framework, Complex Diffusion (CD) is introduced as a regularisation term into the proposed framework that minimizes the noise without blurring edges. Whereas, in the latter strategy a new hybrid regularisation mixture of Complex Diffusion and Shock Filter is used as regularization term. The complex diffusion filter helps in denoising the image and the shock filter helps to retain the basic fine structures and deblurring of the edges. Both the frameworks have been evaluated on both simulated and real standard thorax phantoms. The final results are compared with the other standard methods and it is analyzed that the proposed frameworks have many desirable properties such as better noise robustness, less computational cost, enhanced denoising effect.

Acknowledgements

First, I would like to extend my deep gratitude to my supervisor **Dr. Shailendra Tiwari** for constant supervision, for their advice and patiently guidance at every step of my ME program. Without unfailing support and perception in me, this thesis would now not have been viable. Their contribution to this thesis goes well beyond their role as an academic supervisor and includes constant support on a personal level without which this journey may never have been completed. And for this, I'm truly thankful. He is a great mentor for my life as well.

I would like to express my gratitude to **Dr. Maninder Singh**, Head of Computer Science and Engineering Department and **Dr. Ashutosh Mishra**, P.G. coordinator their constant motivation and encouragement.

I also wish to thank my research committee members and non-teaching staff of the Computer Science and Engineering Department for their help and support. I would also like to thanks to my teachers and friends from whom I learn the art of happiness and never give up approach.

Finally, I would like to express my sincere and deep gratitude to my parents and family member for their love, encouragement, care, and support.

Kavkirat Kaur

Table of Contents

Abstract . . . . . **ii**

Title **Page No.**

Table of Contents . . . . . **iv**

List of Figures . . . . . **vi**

List of Tables . . . . . **ix**

List of Notations . . . . . **x**

List of Abbreviations . . . . . **xi**

Chapter 1 Introduction **1**

1.1 Introduction 1

1.2 Organisation of the Thesis 6

Chapter 2 Foundations of Computed Tomography **7**

2.1 Introduction 7

2.2 Related Work 12

2.3 Datasets Description 16

2.3.1 Test case 1 17

2.3.2 Test case 2 17

2.3.3 Test case 3 18

2.3.4 Test case 4 19

2.4 Quantitative Measures 19

Chapter 3 Problem Statement **22**

3.1 Problem Statement 22

3.2 Motivation 23

3.3 Objective of the Thesis 23

Chapter 4 Proposed Work **24**
4.1 Method and Model for MLEM+CD 24
4.1.1 Proposed Algorithm 28
4.2 Method and Model for Hybrid Regularization 28
4.2.1 Proposed algorithms 32

Chapter 5 Experimental Results **34**
5.1 Experimental Results for MLEM+CD 34
5.1.1 Evaluation based on visualisation 35
5.1.2 Evaluation based on plots 37
5.1.3 Evaluation based on quantitative measures 40
5.1.4 Evaluation based on profile graphs 41
5.2 Experimental Results for Hybrid Regularization 42
5.2.1 Evaluation based on visualisation 43
5.2.2 Evaluation based on plots 45
5.2.3 Evaluation based on quantitative measures 48
5.2.4 Evaluation based on profile graphs 49

Chapter 6 Conclusion and Future Work **51**

References **52**

List of Publications **58**

List of Figures

Figure No.	Title	Page No.
1.1	Classification of various energy sources on the basis of different imaging devices [1]	2
1.2	A classification of different reconstruction methods [1]	4
2.1	Four test phantoms considered in the experimental set up, (a) simulated modified Shepp−Logan head phantom (b) simulated ct phantom (c) simulated elliptical phantom (d) real thorax phantom	16
4.1	Block Diagram of Proposed Model	25
4.2	Block Diagram of Proposed Model	29
5.1	The reconstructed results of Shepp−Logan head Phantom using different methods, (a) original phantom, (b) MLEM (c) MLEM+AD (d) MLEM+TV (e) MLEM+NLM (f) MLEM+AwTV (g) proposed model	35
5.2	The reconstructed results of PET using different methods, (a) original phantom, (b) MLEM (c) MLEM+AD (d) MLEM+TV (e) MLEM+NLM (f) MLEM+AwTV (g) proposed model	36
5.3	The reconstructed results of SPECT using different methods, (a) original phantom, (b) MLEM (c) MLEM+AD (d) MLEM+TV (e) MLEM+NLM (f) MLEM+AwTV (g) proposed model	36
5.4	The reconstructed results of real thorax phantom using different methods, (a) original phantom, (b) MLEM (c) MLEM+AD (d) MLEM+TV (e) MLEM+NLM (f) MLEM+AwTV (g) proposed model	37
5.5	The reconstructed results of Shepp−Logan head phantom using different methods, (a) original phantom, (b) MLEM (c) MLEM+AD (d) MLEM+TV (e) MLEM+NLM (f) MLEM+AwTV (g) proposed model	38

5.6 The reconstructed results of PET using different methods, (a) original phantom, (b) MLEM (c) MLEM+AD (d) MLEM+TV (e) MLEM+NLM (f) MLEM+AwTV (g) proposed model 38
5.7 The reconstructed results of SPECT using different methods, (a) original phantom, (b) MLEM (c) MLEM+AD (d) MLEM+TV (e) MLEM+NLM (f) MLEM+AwTV (g) proposed model 39
5.8 The reconstructed results of real thorax phantom using different methods, (a) original phantom, (b) MLEM (c) MLEM+AD (d) MLEM+TV (e) MLEM+NLM (f) MLEM+AwTV (g) proposed model 40
5.9 (a) Profiles along the middle row of Shepp-Logan phantom (b) Profiles along the middle row of PET phantom (c) Profiles along the middle row of SPECT phantom (d) Profiles along the middle row of original phantom 42
5.10 The reconstructed results of Shepp−Logan head Phantom using different methods, (a) original phantom, (b) MLEM (c) MLEM+AD (d) MLEM+TV (e) MLEM+NLM (f) MLEM+AwTV (g) MLEM+CD (h)proposed model 43
5.11 The reconstructed results of PET using different methods, (a) original phantom, (b) MLEM (c) MLEM+AD (d) MLEM+TV (e) MLEM+NLM (f) MLEM+AwTV (g) MLEM+CD (h) proposed model 44
5.12 The reconstructed results of SPECT using different methods, (a) original phantom, (b) MLEM (c) MLEM+AD (d) MLEM+TV (e) MLEM+NLM (f) MLEM+AwTV (g) MLEM+CD (h) proposed model 44
5.13 The reconstructed results of real thorax phantom using different methods, (a) original phantom, (b) MLEM (c) MLEM+AD (d) MLEM+TV (e) MLEM+NLM (f) MLEM+AwTV (g) MLEM+CD (h) proposed model 45
5.14 Convergence plot of iterations vs. error metrics, (a) PSNR (b) RMSE (c) MSSIM (d) CP for Shepp-Lagon phantom 46

5.15 Convergence plot of iterations vs. error metrics, (a) PSNR (b) RMSE (c) MSSIM (d) CP for PET phantom 47
5.16 Convergence plot of iterations vs. error metrics, (a) PSNR (b) RMSE (c) MSSIM (d) CP for SPECT phantom 47
5.17 Convergence plot of iterations vs. error metrics, (a) PSNR (b) RMSE (c) MSSIM (d) CP for real thorax phantom 48
5.18 (a) Profiles along the middle row of Shepp-Logan phantom (b) Profiles along the middle row of PET phantom (c) Profiles along the middle row of SPECT phantom (d) Profiles along the middle row of original phantom 50

List of Tables

Table No.	Title	Page No.
2.1	Literature Review	12
2.2	Design parameters of the ellipsoids in modified Shepp-Logan head phantom	17
2.3	Design parameters of the ellipsoids in CT test phantom	18
2.4	Design parameters of the ellipsoids in hot and cold test phantom	18
5.1	Quantitative parameters of Shepp-Lagon phantom for test case 1	40
5.2	Quantitative parameters of PET phantom for test case 2	41
5.3	Quantitative parameters of SPECT phantom for test case 3	41
5.4	Quantitative parameters of real thorax phantom for test case 4	41
5.5	Quantitative Parameters of Shepp Lagon head Phantom for Test case 1	49
5.6	Quantitative Parameters of PET Phantom for Test case 2	49
5.7	Quantitative Parameters of SPECT Phantom for Test case 3	49
5.8	Quantitative Parameters of real thorax Phantom for Test case 4	49

List of Notations

f^*	Estimated solution
$E(f)$	Energy functional
λ	Relaxation parameter
$E_1(f)$	Data fidelity
$E_2(f)$	Regularization parameter
f	True image vector
T	Transpose operator
N	Number of voxels
g	Measured data
M	Total number of sampling points
$Im(.)$	Imaginary value
$c(Im(f))$	Diffusion coefficient
k	Threshold parameter

List of Abbreviations

ACOSEM	Accelerated complete-data ordered-subset expectation maximization
AD	Anistropic Diffusion
ADMIRE	Advanced Modelled Image Reconstruction
AEC	Automated Exposure Control
ALARA	As Low As Reasonably Achieved
AMD	Anistropic Median Diffusion
ART	Algebraic Reconstruction Techniques
ASIR	Adaptive Statistical Iterative Reconstruction
AwTV	Adaptive-weighted Total Variation
BICAV	Block Iterative ComponentAveraging
CAV	Component Averaging
CD	Complex Diffusion
CP	Correlation Parameter
CT	Computed Tomography
ECT	Emission Computed Tomography Total Variation
EGAwTV	Edge-guided Adaptive-weighted TV Minimization
EGTV	Edge-guided TV Minimization
EM	Expectation Maximization
EM-TV	Expectation Maximization with Total Variation
ET	Emission Tomography
FBP	Filtered Backprojection
GGMRF	Generalized Gaussian Markov Random Fields
GMRF	Gaussian Markov Random Field
IRIS	Image Space
MAP	Maximum *A Posteriori*
MART	Multiplicative Algebraic Reconstruction Techniques
mAs	Milliampere-second
MBIR	Model-based Iterative Reconstruction
MLEM	Maximum Likelihood Expectation Maximization

MRF	Markov Random Field
MRI	Magnetic Resonance Imaging
MRP	Median Root Prior
MSSIM	Mean Square Similarity Index
NLM	Non Local Means
OSEM	Ordered Subsets Expectation Maximization
PDE	Partial Differential Equation
PET	Positron Emission Tomography
pSART	Polyenergetic SART
PSNR	Peak Signal to Noise Ratio
RAMLA	Row-action Maximum Likelihood Algorithm
RMSE	Root Mean Square Error
SART	Simultaneous Algebraic Reconstruction Techniques
SIR	Statistical Iterative Reconstruction
SIRT	Simultaneous Iterative Reconstruction Techniques
SNR	Signal to Noise Ratio
SPECT	Single Photon Emission Computed Tomography
TV	Total Variation

Chapter 1

Introduction

In this chapter, a brief introduction to the problems of medical image reconstruction considered in this work and basic concepts studied has been presented. In Section 1.1, presents the background of the medical imaging system, In section 1.2, the organization of the thesis is described.

1.1 Introduction

Medical imaging is an emerging technology for performing the diagnosis of diseases using high-resolution cross-sectional images of the internal organs of human body. The advent of advanced computer technology ensures the development of better medical imaging equipment to obtain an accurate functional and anatomical information in a non-invasive way. A dynamic evolution has been observed in the field of medical imaging due to the combined efforts from the interdisciplinary areas of medical, engineering and rudimentary sciences. The main goal of imaging science is to gain convenient and relevant information through the anatomical and functional behaviour of the organs of the human body by using different internal or external sources of energies such as X-Rays, Gamma Waves etc. [1] as shown in Figure 1.1. Before selecting the source of imaging we should know the type of body part that is to be analyzed and what all factors are to be analyzed. In external sources the radiations are passed from the external sources inside the affected body part. Various examples of external sources imaging are X-ray computed tomography, radiography, mammography, ultrasound, Optical Transmission and Transillumination Imaging. In X-ray radiographs, the rays are emitted into the affected body part and depending upon the absorption of the rays the output image is generated. The ultrasound imaging is used for detecting anomalies in soft tissues of the body. In X-Ray Computed Tomography, the image is formed by combining the data taken at different angles of the body part. It is used for the detection of brain tumors, analysis of heart vessels. Whereas in Optical Transmission and Transillumination Imaging the light is passed through for detecting the

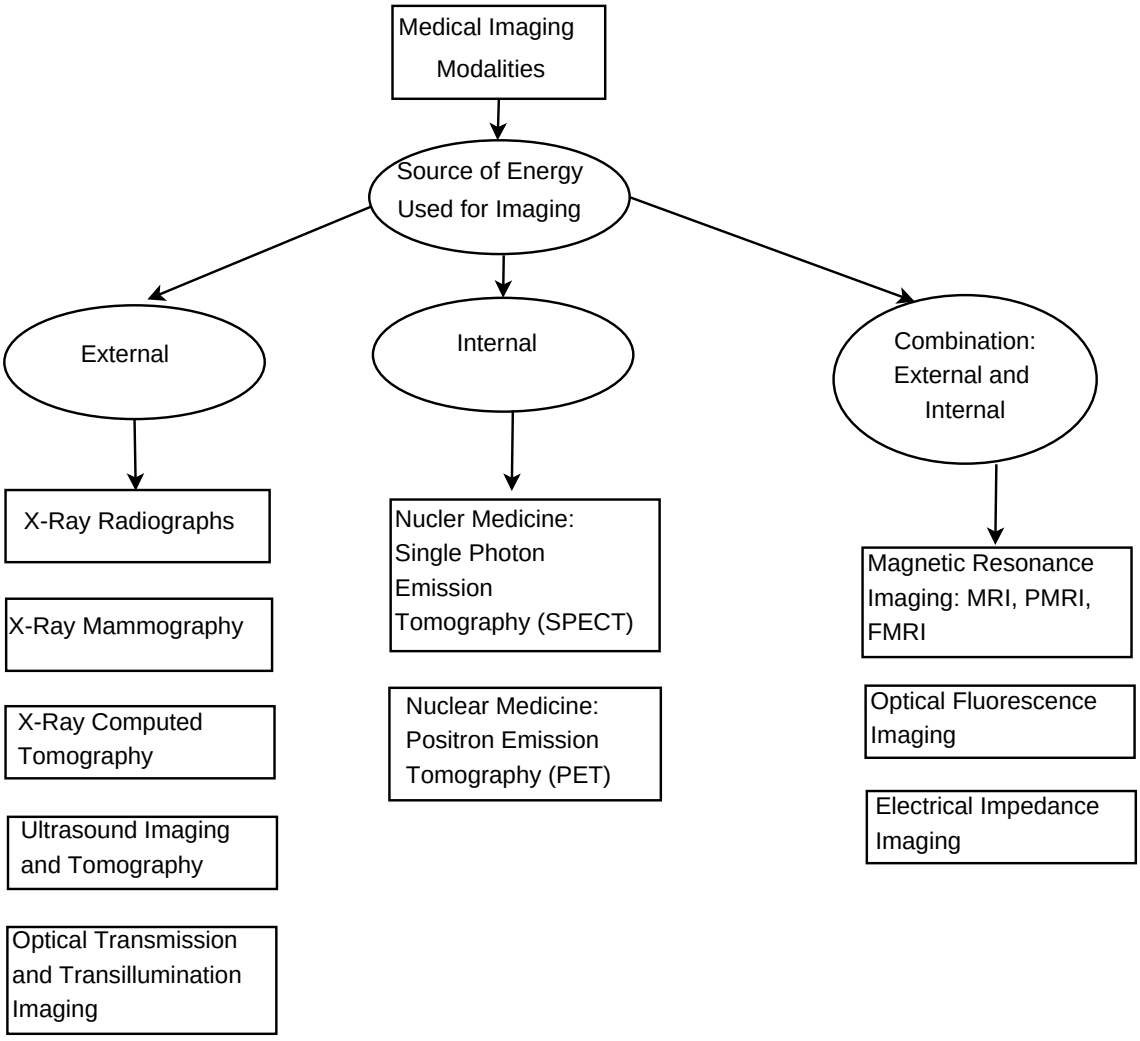

Figure 1.1: Classification of various energy sources on the basis of different imaging devices [1]

anomalies. It is generally used for the detecting problems of infants and children like lung problems, amount of cerebrospinal fluid. In case of internal sources, an radioactive substance is inserted in the particular body portion. Then using the emission imaging principle i.e. the radiations emitted are detected. With the help of this SPECT and PET methods can help to detect the problems related to metabolic processes of body. The last strategy i.e combination of internal and external sources are used to get the fine detailed information about the organs. Magnetic Resonance Imaging uses the concept of combination of internal and external sources. The external source is made to react with a particular atom in the body to make it active which helps in the getting the image.

Though there exist many methods for diagnosis of various disease occurs inside the

human body no one method is fully complete. All these methods are very helpful in medical diagnosis but along with it, they are harmful also. The radiation emitted by the body or by the body both are harmful to the patient. However, excessive use of X-ray radiation may have some harmful effects such as genetic disorder, cancer syndrome and other harmful diseases [2]. So, minimizing the radiations from X-Ray machines has been the major concerned, consequently, low-dose CT is gaining the interest of the researchers.

There are different methods proposed in the past few decades for minimizing the radiation dose [3] are classified into three categories: 1) Minimizing the exposure time and current in the X-ray tube, 2) Decreasing the number of projections, 3) Improving software approaches i.e. the reconstruction methods. In the first method, the reduction of exposure time and current (mAs) is very simple and cost-effective of minimizing the radiations but this method generates noisy projections. Various techniques have been proposed for reducing the exposure time and current (mAs) like Automated Exposure Control (AEC) [4] optimization of the tube potential [4] etc. In the second method, there is a reduction in the number of projection views (angles) during data acquisition i.e. the insufficient amount of projection data due to which the image suffers from artifacts, heavy noise and contrast degradation of soft tissues. However, the third method is related to the improvements of reconstruction algorithms in terms of accuracy, efficiency and robustness. From the last few decades, image reconstruction techniques are essential and intensive research topics in the field of medical imaging. For accurate clinical diagnosis, high-resolution reconstructed images are required from the projection data with the help of efficient and robust algorithms. Generally, CT raw data acquired from the different projection angles were depended upon various factors such as the number of views, radiation dose, camera calibration properties, geometry of the system matrix, duration of the acquisition process, and some external factors based on patient body movements etc.

Hence, many reconstruction algorithms have been developed from the past 30 years which are broadly classified into analytical and iterative methods as shown in Figure 1.2. The analytical techniques were depending upon transformation

techniques such as Radon transform [1, 2]. Filtered back-algorithm (FBP) [5] is one of the most commonly used techniques in this class because of its ability to provide an adequate image quality on the basis of faster, simpler, and computationally efficient manner. Despite, its overall performance, CT studies that the reconstructed images with FBP can be still affected by poor visual quality, staircasing artifacts and less SNR due to the limited projection sets. On the contrary, iterative reconstruction methods have the capability to handle the noisy data and reconstruct a better quality image. Iterative methods have shown a great potential to replace the traditional analytical methods like FBP that was taken into account of statistical properties, which have shown to be superior in suppressing the noise and streak artifacts. In iterative methods, multiple steps have been performed iteratively to form a better quality image. Further, the iterative methods can be divided into iterative methods and statistical iterative methods.

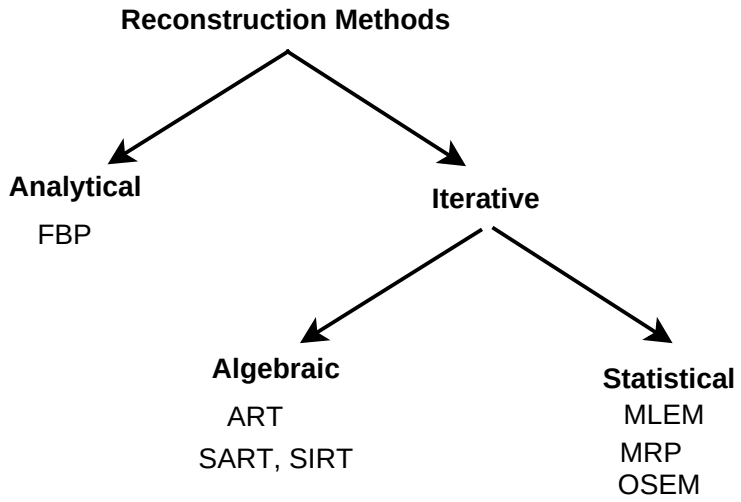

Figure 1.2: A classification of different reconstruction methods [1]

Solving the linear equations is the basic fundamental of algebraic iterative reconstruction techniques. Various algebraic iterative reconstruction techniques are proposed over the period of past years are Algebraic reconstruction technique (ART) [6], Simultaneous iterative reconstructive technique (SIRT) [7], Statistical Algebraic reconstruction technique (SART) [8], Multiplicative algebraic reconstruction technique (MART) [9], Component averaging (CAV) [10], Block iterative component averaging (BICAV) [11], Polyenergetic SART (pSART) [12] and many more

algebraic iterative reconstruction algorithms are present in literature but they all have one common limitation that they produce low quality images and have slow convergence rate.

Statistical Iterative reconstruction (SIR) methods were developed to remove the drawbacks of the previous approaches. SIR methods provide better quality reconstructed images as compared to the algebraic iterative reconstruction methods [13]. Various SIR techniques have been discussed from the past many years are Maximum likelihood expectation maximization (MLEM) [14], Ordered-subset expectation maximization (OSEM) [15], Row-action maximum likelihood algorithm (RAMLA) [16], Accelerated complete-data ordered-subset expectation maximization (ACOSEM) [17], advanced modelled image reconstruction (ADMIRE) [18], Image Space (IRIS) [19], Adaptive statistical iterative reconstruction (ASIR, GE Healthcare) [20], Model-based iterative reconstruction (MBIR) [21]. These all techniques were used to improve the quality of reconstructed images as well as remove artifacts. Among all these techniques MLEM is one of the most commonly used algorithms for the image reconstruction.

All of the SIR methods discussed above are computationally complex and time consuming because it is an inverse problem or ill-posed problem [22, 19, 20] in which we seek to estimate of some unknowns and insufficient quantities. To solve the ill-posedness problem various techniques have been proposed various techniques has been made from last few decades. like smoothing of images with the use various filters [23, 24], defining some sort of stopping rules [25, 24], relaxation of some parameters [21] etc. Among all, maximum a posteriori (MAP) methods are optimal for reducing the noise by using some kind of prior information [24]. MAP methods are combined with SIR to provide better quality and desired results in a significant way. MAP methods are consists of basically two objective functions called as: data fidelity and regularization. In MAP criteria, minimizing the log-likelihood function gives the data fidelity term which portrays the distribution of noise in low dose X-ray CT images [23]. And, regularization is used with the basic SIR algorithms to provide a priori information for better reconstructed images. Numerous edge preserving priors have been used over the past few decades such

as Gaussian mixture priors [26], Gibbs smoothing [27], anisotropic diffusion (AD) [28], total variation (TV) [29], anisotropic median diffusion (AMD) [30], complex diffusion (CD) [31], non-local means (NLM) [32] etc. These priors are known as image-domain-based prior as in these some information is required from the reconstructed images in advance. It is very important to find a suitable prior which fits best with the iterative approach to overcome the limitation of the existing approach.

1.2 Organisation of the Thesis

Throughout the work, the main objective is to design and develop an effective and efficient framework for CT image reconstruction. The overall thesis is organized into six chapters. Chapter 1 provides the introduction to medical imaging. Chapter 2 presents the theoretical background literature survey related to the medical imaging system. In Chapter 3, motivation and problem description for the present work including objectives are discussed. In Chapter 4, to overcome the major drawbacks associated with statistical iterative reconstruction algorithms, two newly proposed methods are discussed. The results of the proposed models are presented in Chapter 5. Finally, in Chapter 6, summarize main findings of this thesis and give future perspectives of the research in this thesis.

Chapter 2

Foundations of Computed Tomography

In this chapter, we have discussed various statistical iterative reconstruction (SIR) methods. All the image reconstruction methods and regularization priors are summarized. In Section 2.1 the basic introduction to medical imaging is explained. In Section 2.2 the literature survey of statistical iterative reconstruction (SIR) methods and regularization priors along with their advantages and limitations is discussed. The description about the datasets used in the work is presented in Section 2.3. The detailed discussion about different performance measures has been discussed in section 2.4.

2.1 Introduction

Today's computed tomography (CT) system has made tremendous growth in the field of imaging science using many applications for accurate clinical diagnosis, detection and modifications over the past few decades. Recent researches in medical science have significantly improvised the perception of scientist and Physician's to better understand the cause of the disease that affects the human system and how the treatment process works behind it. However, excessive use of X-ray radiation may have some harmful effects such as genetic disorder, cancer syndrome and other harmful diseases [2]. So, minimising the radiations from X-ray machines has been the major concerned, consequently, low-dose CT is gaining the interest of the researchers. Generally, ALARA safety (as low as reasonably achieved) principle is used in minimisation of the radiation dose.

There are different methods proposed in the past few decades for minimising the radiation dose [3] are classified into three categories:

1. Minimising the exposure time and and current during the X-ray CT acquisition process.

2. Decreasing the number of projections.

3. Improving software approaches i.e., the reconstruction methods.

In the first method, the reduction of exposure time and current (mAs) is very simple and cost-effective of minimising the radiations but this method generates noisy projections. Various techniques have been proposed for reducing the exposure time and current (mAs) like automated exposure control (AEC) [4] optimisation of the tube potential [4] etc. In the second method, there is a reduction of projection data, acquired from the less number of views (angles) i.e., the insufficient amount of projection data due to which the image suffers from artefacts, heavy noise and contrast degradation of soft tissues. The third method is related to modification and improvements of the efficiency, accuracy and robustness of image reconstruction algorithms. Thats why in this work, the third method is taken in our consideration to proceed towards the achievement of the proposed approach.

In literature, there are various methods of image reconstruction that are introduced over the last few decades. Basically, they are broadcasted in two main categories [24] i.e., analytical reconstruction and iterative reconstruction. In analytical reconstruction, filtered back propagation (FBP) [5] is the standard algorithm for image reconstruction from past many decades and is used due to its computational efficiency and numerical stability. Generally, the poor quality images are constructed by the analytical method as greater noise is induced during data acquisition when amount of radiation is reduced. Despite of, iterative method has the capability to handle the noisy data and reconstruct a better quality image. Iterative Reconstruction methods have shown great potential to replace traditional analytical methods like FBP that was taken into account of statistical properties, which have shown to be superior in suppressing the noise and streaking artifacts [33]. Iterative reconstruction methods are computationally more expensive than analytical reconstruction. In Iterative reconstruction, multiple steps are performed iteratively to form a better quality image.

Iterative reconstruction is further categorised into two types algebraic and statistical iterative reconstruction (SIR) methods. Solving the linear equations is the basic fundamental of algebraic iterative reconstruction techniques. Various

algebraic iterative reconstruction techniques are proposed over the period of past years. Algebraic reconstruction technique (ART) [6] method repeatedly changes the structure until it satisfies with the original one. Simultaneous iterative reconstructive technique (SIRT) [7] is the advancement of ART method, the densities are altered with respect to all the angles of projections which help in improving the results. Andersen and Kak [8] proposed an algorithm which can consider to be the best combination of ART and SIRT termed as statistical algebraic reconstruction technique (SART). As it is imposing the higher convergence rate property of ART and noise-reducing property of SIRT. In SART all the acquired pixels updates for only one view at a time. After that the concept of Multiplicative algebraic reconstruction technique (MART) was introduced by Mishra et al. [9] to maximises the entropy and confining the image. Component averaging (CAV) [10] was a technique proposed that can handle large linear equations parallel. Block iterative component averaging (BICAV) [11] optimises some parameters of CAV for better results. Polyenergetic SART (pSART) [12] was introduced to reduce beam hardening artefacts and improve the CT images. There are many more algebraic iterative reconstruction algorithms present in literature but they all have one common limitation that they produce low quality images and have slow convergence rate.

SIR methods were developed to remove the drawbacks of the previous approaches. SIR methods provide better quality reconstructed images as compared to the algebraic iterative reconstruction methods [13]. Various SIR techniques have been discussed from the past many years. Maximum likelihood expectation maximisation (MLEM) [14] generating a better quality image by smoothing an image but is affected by the problem of slow convergence rate. To provide fast convergence rate the ordered subset projection data was merged with MLEM and termed as ordered-subset expectation maximisation (OSEM) [15]. Row-action maximum likelihood algorithm (RAMLA) [16] is similar to OSEM, it also works on the subsets and has less computational cost, more accurate as compared to OSEM. Accelerated complete-data ordered-subset expectation maximisation (ACOSEM) [17] method is the enhancement of OSEM by accelerating the speed by two times using the optimised parameters. Gordic et al. [18] proposed advanced modelled image re-

construction (ADMIRE) which has the capability of providing better image quality both at the standard as well as low dose levels. Later, image reconstruction in image space (IRIS) [19], the virtual image is created from raw data which increases the processing time and reduces noise. Adaptive statistical iterative reconstruction (ASIR, GE Healthcare) [20] was one of the first IR algorithm that was clinically accepted for low radiation dose. Another technique, model-based iterative reconstruction (MBIR) [21] is a promising and advanced reconstruction method than ASIR that could improve CT image quality with low radiation dose and remove streak artefacts. MBIR is capable of producing an image with same quality by allowing further reduction of radiation dose. These all techniques were used to improve the quality of reconstructed images as well as remove artefacts. Among all these techniques MLEM is one of the most commonly used algorithms for the image reconstruction.

All of the SIR methods discussed above are computationally complex and time consuming because it is an inverse problem or ill-posed problem [22, 19, 20] in which we seek to estimate of some unknowns and insufficient quantities. To solve the ill-posedness problem various techniques have been proposed in literature over the past few decades like smoothing of images with the use various filters [23, 24], defining some sort of stopping rules [25, 24], relaxation of some parameters [21] etc. Among all, maximum a posteriori (MAP) methods are optimal for reducing the noise by using some kind of prior information [24]. MAP methods are combined with SIR to provide better quality and desired results in a significant way. MAP methods are consists of basically two objective functions called as: data fidelity and regularisation. In MAP criteria, minimising the log-likelihood function gives the data fidelity term which portrays the distribution of noise in low dose X-ray CT images [24]. And, regularisation is used with the basic SIR algorithms to provide a priori information for better reconstructed images.

Numerous edge preserving priors have been used over the past few decades such as Gaussian mixture priors [26], Gibbs smoothing [27], anisotropic diffusion (AD) [28], total variation (TV) [29], anisotropic median diffusion (AMD) [30], complex diffusion (CD) [31], non-local means (NLM) [32] etc. These priors are known

as image-domain-based prior as in these some information is required from the reconstructed images in advance. It is very important to find a suitable prior which fits best with the iterative approach to overcome the limitation of the existing approach. Up to now, MLEM with AD named as MLEM-PDE has been proposed by Yan [34]. In his work, he uses the Perona and Malik (P-M) diffusion model and due to its defects unable to minimize the noise as well as preserve the sharp edges. Also, MLEM with AD requires more number of iterations. Bhadauria and Dewal [35] performed an analysis on the various regularisation priors namely, Wiener filter, Median filter, AD, wavelet-based method, TV and it is observed that the fine details of the images are not preserved, blurring effects and edges are not preserved. AMD is an improved version of the AD which provides better smoothing. Later, He and Huang [36] proposed a model MLEM-AMD which is the combination of MLEM and AMD as regularisation term. This model provides better results than MLEM-PDE but still face problem in detecting the edges. Zhang et al. [24] proposed NLM as regularisation term with SIR. But this approach is very time consuming and complex approach Chavez-Rivera et al. [37]. TV is considered to be a good approach for the reduction of noise from the image. Besides of a good approach, sometimes edges are considered as the noise and are removed due to which the results of the reconstructed image decrease. A new concept of kernel-based regularisation was proposed by Boudjelal et al. [38] termed as (k-MLEM) which has an additional capability of removing the background noise from the image.

It has been shown that reduction of radiation dose during data acquisition gives rise to the Gaussian noise which is due to the intrinsic nature of electronic fluctuations. It means that projection data acquired by low energy radiation were considered to follow a signal independent Gaussian distribution [39, 40]. Therefore, it is required to design a filter that can handle the noise effect efficiently and preserve the edges that lead to maximising the crucial diagnostic information. It is the dire need of the day to review efficacy of the regularisation term for smoothing purpose [40, 24]. However, a variety of high order denoising techniques have been developed [34, 36, 2, 37] from the past few decades, still one of the common problem associated with regularisation term is to over smooth an image or its

gradient may lead to blurring the edges, staircase effect, loss of region-of-interest (ROI) and meaningful informations.

2.2 Related Work

Table 2.1: Literature Review

Sr No	Papers	Description	Advantages	Limitations
1.	Maximum Likelihood Reconstruction for Emission Tomography. (Shepp and Vardi, 1982) [41]	It gives an accurate mathematical model for Emission Tomography (ET) based on the inverse problem where emission intensity depends upon the number of photon counts and detector units.	In this model, value of lambda is the calculated which that maximizes the probability depending upon the number of photon counts and detector units.	It doesn't specifies a prior that leads to a more computationally feasible solution for PET.
2.	Bayesian reconstructions from emission tomography data using a modified EM algorithm. (Green, 1990) [22]	In this paper, new technique of reconstruction for SPECT data is proposed based on EM approach to maximize the likelihood of reconstructed ET data.	A novel method for EM algorithm is proposed which practically feasible and provides smoothness in the output.	It manually set the value of controlling parameter beta.
3.	Bayesian image reconstruction for emission tomography based on median root prior. (Anius and Ruotsalainen 1997) [42]	Median root prior (MRP) based a new Bayesian one-step-late (OSL) reconstruction algorithm is proposed. It works on local monotonous radioactive concentrated images, various	The proposed MRP method performed well both quantitatively and qualitatively with a similar resolution to the FBP method with ramp filter and MLEM methods.	The beta values was set manually, it gives good result on smaller value of beta and for higher values still the noise was present.

Table 2.1: Literature Review

Sr No	Papers	Description	Advantages	Limitations
		dataset and some patient examinations with PET.		
4.	Investigation of positron emission tomography image reconstruction (Yan, 2007) [34]	The anisotropic diffusion filter introduced by Perona and Malik was merged with MLEM as regularization prior for denoising the image.	Provides better results as compared to the standard MLEM algorithm. High PSNR value.	Due to its defects unable to decrease the noise and retain the edges. Also needs more number of iterations.
5.	Low Dose CT Reconstruction via Edge-preserving Total Variation Regularization (Tian et al. 2011) [43]	The edge preserving Total Variation term was used as a regularization term to preserve the sharp and minor edges.	The proposed method perform better than the TV-based algorithm and conventional FBP algorithm. It reduces the noise for the low dose radiation and minimize the streaking artifacts.	GPU is used but still speed of this iterative method can't compete the speed of FBP. Efficiency of algorithm should be improved.
6.	Adaptive-weighted total variation minimization for sparse data toward low-dose x-ray computed tomography image reconstruction (Liu et al. 2012) [44]	The proposed AwTV model was derived by considered the anisotropic edge property among neighboring image voxels.	The proposed methods shows the better results with several benefits like: noise-resolution tradeoff plots, full-width at half-maximum values, preserving edges.	The Convergence speed was similar to the TV-POCS model. It needs different data constraints for different applications.
7.	Comparative evaluation of denoising methods on brain CT images (Bhadauria and	An analysis on the various regularization priors such as Wiener filter, Total variation	The wavelet based method attains the higher PSNR value than all other models.	TV method does not preserve the fine particles, blurry effects. Wavelet

Table 2.1: Literature Review

Sr No	Papers	Description	Advantages	Limitations
	Dewal 2013) [35],	(TV), Anisotropic Diffusion (AD) filter, Median and some wavelet based filters.	Provides better results by denoising the image.	method does not help to retain the edges.
8.	Penalized Maximum Likelihood Algorithm for Positron Emission Tomography by Using Anisotropic Median− Diffusion (Qian He, 2014) [36]	In proposed algorithm, anisotropic median diffusion (AMD) filter is fused with maximum likelihood expectation maximization (MLEM) algorithm for improving the quality of PET images.	The fusion algorithms significantly improves the image reconstruction methods and produced high quality reconstructed images.	Though it provides better results than MLEM but still unable to retain the edges, preserves structures and suffer from fine stair casing effects.
9.	Superiorization of the MLEM algorithm (Garduno and Herman, 2014) [25]	A superiorization methodology is applied to MLEM. The proposed approach is based on combination of Gaussian and Total variation approach.	The proposed method outperforms than MLEM and other iterative methods using the statistical hypothesis test and simulated PET data of head phantom.	Choice of optimum initial point; do not preserve the fine particles.
10.	Statistical image reconstruction for low-dose CT using nonlocal means-based regularization.(Hao et al. 2014) [3]	In this algorithm, nonlocal means (NLM) filter based is used with SIR method to reconstruct the images using low radiation dose and current (mAs) during CT acquisition	This method can achieve more significant gains on the basis of noise reduction without losing the image details.	The proposed method cannot effectively remove the noise, stair-case artifacts and the computational time is more.

Table 2.1: Literature Review

Sr No	Papers	Description	Advantages	Limitations
		process.		
11.	Statistical image reconstruction for low-dose CT using nonlocal means-based regularization. Part II: An adaptive approach (Zhang et al. 2014) [24]	To remove the drawbacks of NLM regularization, a novel method is proposed based on the tuning of adaptive spatial filter parameters for high quality reconstructed images.	The proposed method shows the necessity of spatially variant filter and improve the efficiency of reconstructed images for low dose acquisitions.	The size of search-window and patch-window don't show any clear effect on the reconstructed image. Parameters tuning is not optimal
12.	MLEM reconstruction model including total variation for low dose pet high resolution data (Chavez-Rivera et. al., 2015) [37]	The proposed method uses Total Variation (TV) as a prior term with Expectation Maximization (EM) iterative method called as (EM-TV) under Bayesian framework.	MLEM-TV significantly improves the image quality and accuracy in comparison with that obtained using MLEM from low number of counts.	The limitation is that the TV method does not preserve the fine particles.
13.	An adaptive nonlocal filtering for low-dose CT in both image and projection domains (Yingmei Wang et at., 2015) [45]	The proposed method smooth the noisy sinogram space data using non-local filtering techniques and then reconstruct the image by simple filtered back-projection (FBP) algorithm.	The proposed method tremendously improve the quality of reconstructed images in low-dose CT data.	The proposed method is computationally complex and has taken more time during reconstruction therefore it needs to further optimize the parameters.
14.	CT reconstruction from few-views with anisotropic edge-guided (Junyan	The Proposed method uses adaptive Total Variation (AwTV) filtering scheme	The proposed method significantly smooth and recover the weak edges and provide better	Choice of optimum initial point and stopping can be adaptive criteria.

Table 2.1: Literature Review

Sr No	Papers	Description	Advantages	Limitations
	total variance Rong et. at., 2016) [46]	during energy minimization framework called as edge-guided AwTV i.e. (EGAwTV) method.	reconstructed CT images on few-view projection data.	
15.	A Novel Kernel-Based Regularization Technique for PET Image Reconstruction (Boudjelal et.al.,2017) [38]	In this proposed algorithm, box-kernel technique is coupled with basic MLEM iterative reconstruction method called as k-MLEM.	On comparing with standard MLEM, it removes noise and artifacts, preserves edges effectively.	Slow converge rate; time consuming;

2.3 Datasets Description

To validate the performance of the proposed approach four test cases phantoms have been considered in this work shown in Figure 2.1.

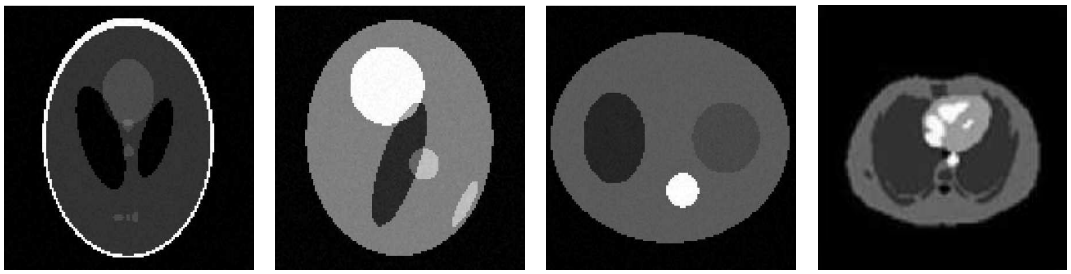

(a) (b) (c) (d)

Figure 2.1: Four test phantoms considered in the experimental set up, (a) simulated modified Shepp−Logan head phantom (b) simulated ct phantom (c) simulated elliptical phantom (d) real thorax phantom

Out of the four test cases, three are computer generated (simulated) CT phantoms and one is real medical thorax CT phantom. The description of all the four test phantom (such as the design parameters for the simulated test phantoms) has been presented separately as follows:

2.3.1 Test case 1

In simulated test case 1, the modified Shepp-Logan head phantom (shown in Figure 2.1a) has been considered having a size of 128×128 pixels. This phantom is commonly used to conduct a simulated experiment for a variety of medical imaging applications. It solely consists of ellipses of differing size, shape, orientation, and intensity, super-positioned on one another. To design the mathematical phantom, we set up an imaging geometry using parallel-beam CT scanner and use a circular rotation to acquire 90 projection views uniformly distributed over 360°, where, each projection view contains at least 150 measurements. The system matrix $a_{ij}$is calculated by the geometric calibration method [47] of the pixels. In a practical scenario, it is almost impossible to obtain the noise free projections during CT imaging process, even though we increase the radiation dose. Therefore, 10% of Gaussian random noise with zero mean and 0.1 times variance is added to validate the robustness of the proposed method during image reconstruction.

Table 2.2: Design parameters of the ellipsoids in modified Shepp-Logan head phantom

Centre coordinates of ellipses (x_0, y_0)	Horizontal and vertical length of semi axis of ellipses (a, b)	Angles between the semi-axis (phi)	Additive intensity value of the ellipses (A)
$(0, 0)$	$(0.69, 0.92)$	0	1
$(0, 0.0184)$	$(0.6624, 0.8740)$	0	0.8
$(0.22, 0)$	$(0.1100, 0.3100)$	18	0.2
$(0.22, 0)$	(0.1600,0.4100)	18	0.2
(0,0.35)	(0.2100,0.2500)	0	0.1
(0,0.1)	(0.0460,0.0460)	0	0.1
(0,0.1)	(0.0460,0.0460)	0	0.1
$(0.08, 0.605)$	(0.0460,0.0230)	0	0.1
$(0, 0.606)$	(0.0230,0.0230)	0	0.1
$(0.06, 0.605)$	(0.0230,0.0460)	0	0.1

2.3.2 Test case 2

In Test case 2, the mathematically simulated CT test phantom [shown in Figure 2.1b] has been considered having a size of 128×128 pixels. It is made up of five different size ellipses with various parameter values as shown in Table 2.3. This

Table 2.3: Design parameters of the ellipsoids in CT test phantom

Centre coordinates of ellipses (x_0, y_0)	Horizontal and vertical length of semi axis of ellipses (a, b)	Angles between the semi-axis (phi)	Additive intensity value of the ellipses (A)
(0.8,0.95)	(0,0)	0	0
(0.75,0.90)	(0,0)	0	0.5
(0.30,0.30)	(0.10, 0.40)	0	0.5
(0.15,0.50)	(0, 0.20)	0	0.35
(0.12,0.12)	(0.2, 0.20)	0	0.25
(0.05,0.20)	(0.53, 0.50)	0	0.25
(0.12,0.50)	(0, 0.12)	0	0
(0.25,0.05)	(0.25, 0.54)	0	0
(0.27,0.05)	(0.27, 0.54)	0	0
(0.20,0.30)	(0.35, 0.20)	-20	0

phantom represents a physiological, electrical and metabolic activity of the brain's anatomy. The total number of projection count value was 6×10^5 and the other designing parameters are exactly similar to the test case 1.

2.3.3 Test case 3

In test case 3, the computer-based simulated projection data attenuated by parallel beam projections, called the elliptical phantom [shown in Figure 2.1c] has been considered having a size of 128×128 pixels. The dimensions of the elliptical phantom are 128 cm, 48.2 cm, and 32 cm respectively and other designing parameters that describe varying intensity of cross-section area of a patient chest body are shown in Table 2.4. The different size of ellipses shown in Table 2.4 signifies the

Table 2.4: Design parameters of the ellipsoids in hot and cold test phantom

Centre coordinates of ellipses (x_0, y_0)	Horizontal and vertical length of semi axis of ellipses (a, b)	Angles between the semi-axis (phi)	Additive intensity value of the ellipses (A)
(0,0)	(0.96,0.80)	0	0.5
(0.35,0.45)	(0.25,0.35)	0	0.3
(0.27,0.45)	(0.27,0.27)	0	0.1
(0.10,0.40)	(0.13,0.13)	0	0.9

low, as well as high activities of the lungs, correspond to the myocardium. The projection data were obtained with CT geometry to calculate the intensity of the

pixels at different view angles. The projection views of these angles are set as 30, 60, 90 and 120 degrees, sampled evenly over 180 degrees, respectively. Also, there are 150 detectors at each projection view.

2.3.4 Test case 4

The fourth test case is a standard real thorax phantom data (shown in Figure 2.1d) acquired from Siemens CT machine. The size of the phantom is 128×128 pixels, similar to other test phantoms considered in this work. The phantom was scanned by clinical CT scanner having parameter setting as: tube voltage set at 120kVp, exposure level set at 100 mAs, the radius of source circle set at 2.868 mm, ray spacing of 1.2 mm, and the distance between the source and detector band from the centre was 408 mm and 816 mm, respectively.

2.4 Quantitative Measures

For the evaluation of the performance of the proposed approach in both quantitative and visual manner, different quality measures like peak signal-to-noise ratio (PSNR), the root mean square error (RMSE), mean structure similarity index map (MSSIM) and the correlation parameter (CP) have been considered which are discussed below:

1. PSNR: PSNR is most commonly used to measure the quality, noise reduction of the reconstructed image [48]. The mathematical formulation of PSNR is as follows:

$$\begin{aligned} &PSNR\%(f_{REC}, f_{ORIG}) \\ &\quad = 10 \log 10 \frac{max^2(f_{ORIG})}{\sum_{x=1}^{M} \sum_{y=1}^{N} [f_{REC}(x,y) - f_{ORIG}(x,y)]^2} \times 100\% \end{aligned} \tag{2.1}$$

   where $f_{ORIG}(x,y), f_{REC}(x,y), and \bar{f}$ denotes the original image, reconstructed image, and the average gray scale of all pixels in the reconstructed image, respectively. Higher is the PSNR value, greater is the quality of the reconstructed image.

2. RMSE: It is a commonly used performance measurement to calculate the

difference between the reconstructed image and the ground truth image [48] and is given as:

$$RMSE\%(f_{REC}, f_{ORIG}) = \sqrt{\frac{\sum_{x=1}^{M}\sum_{y=1}^{N}[f_{REC}(x,y) - f_{ORIG}(x,y)]^2}{J^2}} \times 100\% \tag{2.2}$$

where $f_{REC}(x, y)$ and $f_{ORIG}(x, y)$ denotes the pixel value of the reconstructed and the ground truth image. And, the total number of pixels in the image is denoted by J. Theoretically, it is assumed that the efficiency of the reconstructed algorithm depends upon the minimum value of Root mean square error.

3. MSSIM: The structural similarity index map (SSIM) is human visual system (HVS)-based quality measure. It calculates the degree of similarity between two images provided which one of the images has acceptable quality. SSIM is used on the synthetic CCD noise compensated image to calculate the similarity between the original image and the processed image based on three parameters viz. luminance, contrast, and small structure [48]. The following expression is used to calculate the MSSIM using the formulation for the original image $f_{ORIG}(x, y)$ and the reconstructed image $f_{REC}(x, y)$:

$$MSSIM\%(f_{REC}, f_{ORIG}) = \frac{1}{M}\sum_{j=1}^{M}(x_i, y_j) \times 100\% \tag{2.3}$$

$$SSIM\%(x, y) = \frac{(2\mu_x\mu_y + C_1)(2\sigma_{xy} + C_2)}{(\mu_x^2 + \mu_y^2 + C_1)(\sigma_x^2 + \sigma_y^2 + C_2)} \tag{2.4}$$

where the constant C_1 and C_2 are used to avoid instability when the local means x and y or the standard deviations σ_x and σ_y are very close to zero. The value of MSSIM equal to 1 indicates perfect similarity with the original image.

4. CP: It is commonly used for edge preservation or sharpness [48]. It suppresses the noise or streak artefacts and also preserves the edges of the original image simultaneously. To evaluate the performance of the edge

preservation or sharpness, the CP is defined as follows:

$$CP(f_{REC}, f_{ORIG}) = \frac{\sum_{x=1}^{M}\sum_{y=1}^{N}(f_{ORIG}(x,y) - \hat{f}_{ORIG}(x,y) \times (f_{REC}(x,y) - \hat{f}_{REC}(x,y)}{[\sum_{x=1}^{M}\sum_{y=1}^{N}(f_{ORIG}(x,y) - \hat{f}_{ORIG}(x,y)^2 \times (f_{REC}(x,y) - \hat{f}_{REC}(x,y)^2]^{1/2}} \tag{2.5}$$

where $f_{ORIG}(x,y)$ and $f_{REC}(x,y)$ refers to the pixel value of the ground truth image and the reconstructed image, respectively, similarly the notations $\hat{f}_{ORIG}(x,y)$ and $\hat{f}_{REC}(x,y)$refers to the average value of the original image and the reconstructed image, respectively, via a 3×3 neighbourhood of the standard Laplacian filter. To check the optimal effect of edge preservation, the value of CP should be close to unity.

5. SNR: It is defined as the ratio of the power of the signal (meaningful information) and the power of background noise (unwanted signal) [48]. The mathematical formulation of SNR is as follows [49]:

$$SNR(f_{REC}, f_{ORIG}) = 10\log 10\frac{\sum_{x=1}^{M}\sum_{y=1}^{N}[f_{REC}(x,y) - \bar{f}]^2}{\sum_{x=1}^{M}\sum_{y=1}^{N}[f_{REC}(x,y) - f_{ORIG}(x,y)]^2} \times 100\% \tag{2.6}$$

where f_{ORIG}, f_{REC} and f denotes the original image, reconstructed image, and the average gray scale of all pixels in the reconstructed image, respectively. Higher is the SNR value, greater is the quality of the reconstructed image.

Chapter 3

Problem Statement

In this chapter, we have discussed problem statement and research gaps. Rest of the work is organized as follows: Section 3.1, present the Problem Statement of the work. Section 3.2 presents the motivation behind the work. Finally, section 3.3 presents the objective of the work.

3.1 Problem Statement

The main problem faced during the reconstruction of medical images is in the image formation process in which image formed by combining several raw data measurements of the energy/radiation around the body of a patient. This is an ill-posed problem to which an output may or may not exist because of excessive noise, or the output may not be unique. The primary issue of an inverse problem is related to the fact that the required body portion is not directly available for measurements. The data collected from the scanners is not complete and is not accurate (statistical noise), which leads to the reconstruction of the blurred images with some streaking artifacts. This is a time consuming process and results in blurred and undefined boundaries, loss of fine structures, and may mislead while diagnosing the disease. So to overcome the problem of incomplete data, our goal is to develop a new modified statistical iterative reconstruction algorithms. The development that we aim is associated with both speed of reconstruction and the quality of the reconstructed image. Another main issue is the radiation dosage the patient receives during a scan. The radiation dose and the quality of the image both are directly proportional to each other i.e low amount radiations leads to the production a lower quality image with excessive noise while high dose of radiations generates better image quality. But, these radiations are harmful, hence there is a dire need to improve the quality of an image with low radiations with help of advanced reconstruction strategies. Advanced reconstruction strategies help to reduce the noise and generate high quality images. With this, the patients are less exposed to radiations with proper diagnosis.

3.2 Motivation

The motivation behind this work presented in this thesis is the medical application of Computed tomography (CT). CT is used in clinical diagnosis to detect abnormalities such as cancer, tumors, or organ deficiencies. The development and design of an efficient framework for the medical image reconstruction is one of the challenging problems in medical imaging. With the emergence of various medical imaging modalities for the diagnosis of diseases in the internal organs of the human body, image reconstruction algorithms become a major role to obtain a high quality reconstructed image. This concept needed for research and implementation of statistically based iterative reconstruction methods are spread far and wide over the literature, in journals with homes in engineering, mathematics, physics, radiology, and statistics. This thesis deals with the comparison of various iterative reconstruction methods.

3.3 Objective of the Thesis

The main objective of the work is to investigate and present the quantitative analysis of various regularization priors available in reconstruction literature and to overcome the problem of ill-posedness and recommendation for selecting an appropriate prior to be used with Statistical Iterative reconstruction (SIR). The success of efficient framework for medical image reconstruction relies to handle the issue of ill-posedness by using suitable regularization term, and sharpening the edges as well as to improve the quality of reconstructed images. The improvement that we aim is related to both speed of reconstruction and the quality of the obtained image.

Chapter 4

Proposed Work

In this chapter, to overcome the major drawbacks associated with statistical iterative reconstruction algorithms which include the problem of blurring of the edges, staircase effect, loss of basic fine structure and detailed information. We have proposed two new models. Rest of the work is organized as follows: Section 4.1, present the theoretical background and the first proposed model. Section 4.2 presents the theoretical background and the second proposed model.

4.1 Method and Model for MLEM+CD

The main problem of low−dose CT image reconstruction considered in this work is an ill-posed problem either due to the scarcity of X-Ray projections data or due to the presence of noise and other inconsistencies in the acquired sinogram CT data [37]. Therefore, the image estimation that directly optimizes the maximum likelihood (ML) criterion can be very noisy and unstable. So researchers reformulate this problem with the MAP estimation by applying a prior term to penalize the solution. The prior term enables us to incorporate available information or expected properties of the image to be reconstructed. P-M has introduced the first partial differential equation (PDE) based on nonlinear AD filter [28]. Although this method can retain the edges to some amount, it cannot retain the edge details effectively for very noisy images. It also causes the blocking staircase effect in the final outcome. In addition to that, it leads to smoothening out only the strong magnitude edges that affect over smoothing and lost fine edges. Therefore, to preserve the minor information as well as to produce the quality images, more robust regularisation is needed. Here, in this work, a new nonlinear CD [31] prior is introduced as a regularisation term in CT image reconstruction to reduce the limitations of AD method. The CD prior consists of two terms real part and an imaginary part which behaves as a real diffusion process and a second order derivative of the real part, respectively. In CD the imaginary part is used as the stopping criteria which help to remove the noise and overcome the staircase effect

produced in AD. The imaginary part also plays an important role in better edge detecting. The free Schrdinger equation is combined with a diffusion equation of a complex domain by Gilboa et al. (2004) to form a nonlinear CD with a complex value diffusion coefficient. The block diagram for the proposed model is shown in Figure 4.1

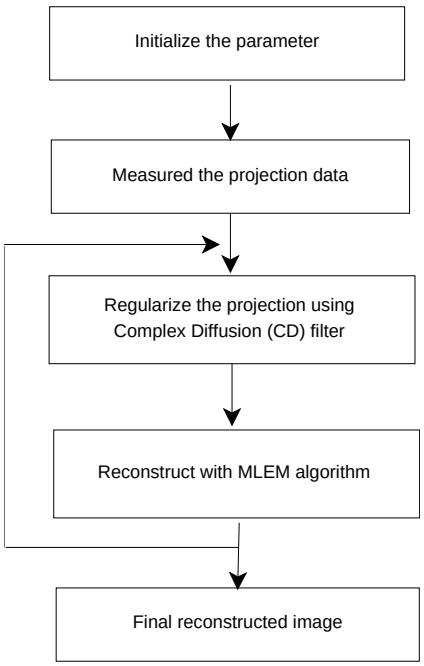

Figure 4.1: Block Diagram of Proposed Model

Here, we incorporate nonlinear CD filter as a regularisation term with SIR method for low dose image reconstruction. The reconstructed image can be achieved by minimizing the cost function. In variational framework [24, 47] the minimisation problem can be read as:

$$f^* = \arg\min_{f \geq 0} E(f) \tag{4.1}$$

where f^* is the estimated solution i.e., the reconstructed image obtained by minimizing the energy functional $E(f)$, with constraints that all values of f must be positive. To solve the optimization problem of equation 4.1, could be equivalently written as:

$$E(f) = E_1(f) + \lambda E_2(f) \tag{4.2}$$

In equation (4.2), $E_1(f)$ is called as a data fidelity term that models the statistic of measured projection data whereas the second term represents the regularisa-

tion or smoothing term which is used as a priori knowledge of the image to be reconstructed. The balancing parameter is used to control the trade-off between data fidelity and regularisation.

In the noisy environment, the normal (Gaussian) probability distribution function (PDF) of the measured projection data is given by:

$$P(g|f) = \prod_{i=1}^{M} P(g_i|f_i) = \prod_{i=1}^{M} \frac{1}{\sqrt{2\pi\sigma_i^2}} \exp(-\frac{(g_i - f_i)^2}{2\sigma_{y_i}^2}) \tag{4.3}$$

where $f = (f_1, f_2, , f_N)^T$ represents the true image vector to reconstruct the image, T represents the transpose operator, N is the number of voxels, $g = (g_1, g_2, ..., g_M)^T$ is the measured data, $M$is the total number of sampling points in the projection data. $P(g|f)$ is the probability of the detected measurement vector g with image intensity f. By taking the negative log-likelihood of the approximated data after elimination of constant and irrelevant terms results in the function is given by:

$$E_1(f) = \ln P(g|f) = \Sigma_{i=1}^{M} \{\frac{(g_i - f_i)^2}{2\sigma_{y_i}^2}\} \tag{4.4}$$

In the MAP estimation, the regularisation is used as *priori* information aiming to provide the solution of the ill-posedness problem in the reconstruction algorithm images [44]. Since the ideal requirement for any regularisation term is to achieve the optimal reconstructed image with preserved features while keeping low radiations, a robust regularisation method is required. Therefore, we choose a nonlinear CD regularisation term due to the following reason:

a) It preserves the edges and minor information in the noisy projection data

b) It provides the reconstructed image in an acceptable computational time.

Thus, the regularisation function can be written as:

$$E_2(f) = \arg\min(div(c(Im(f))\nabla f)) \tag{4.5}$$

where $Im(.)$ is the imaginary value and the diffusion coefficient $c(Im(f))$ is defined

as:

$$c(Im(f)) = \frac{\exp(i\theta)}{1 + (\frac{Im(f)}{k\exp(i\theta)})^2} \tag{4.6}$$

where k is defined as threshold parameter. The value of phase angle θ must be less than one i.e., ($\theta << 1$). The results of the proposed framework can be acquired by substituting equations (4.4) and (4.5) into equation (4.2), to get the modified energy function written as:

$$E(f) = \arg\min_{f \geq 0} E(f) = \Sigma_{i=1}^{M} \{ \frac{(g_i - f_i)^2}{2\sigma_{y_i}^2} \} + \lambda \int_{\Omega} (div(c(Im(f))\nabla f)) d\Omega \tag{4.7}$$

The functional $E(f)$ is defined on the set of $f \epsilon BV(\Omega)$ such that $\log f \epsilon L^1(\Omega)$ and f must be positive everywhere.

$$f^* = \Sigma_{i=1}^{M} \{ \frac{(g_i - f_i)^2}{2\sigma_{y_i}^2} \} + \lambda div(c(Im(f))\nabla f), \ with \ \frac{\partial f}{\partial \vec{n}} = 0 \ on \ \partial\Omega \tag{4.8}$$

The consideration of Euler-Lagrange minimization technique combined with the gradient descent approach provides the optimum solution which given by:

$$f^* = \frac{(g_i - f_i)}{\sigma_i^2} + \lambda div(c(Im(f))\nabla f), \ with \ \frac{\partial f}{\partial \vec{n}} = 0 \ on \ \partial\Omega \tag{4.9}$$

For digital implementations, the equation (4.9) can be discretised using finite differences schemes [47]. After discretisation, the proposed model reads as:

$$\frac{f_j^{\hat{t+1}} - f_j^{\hat{t}}}{\Delta t} = \frac{(g_i - f_i)}{\sigma_i^2} + \lambda div(c(Im(f_j^{\hat{t}}))\nabla f_j^{\hat{t}}), \ with \ \frac{\partial f}{\partial \vec{n}} = 0 \ on \ \partial\Omega \tag{4.10}$$

$$f_j^{\hat{t+1}} = f_j^{\hat{t}} + \Delta t[\frac{(g_i - f_i)}{\sigma_i^2} + \lambda div(c(Im(f_j^{\hat{t}}))\nabla f_j^{\hat{t}})], \ with \ \frac{\partial f}{\partial \vec{n}} = 0 \ on \ \partial\Omega \tag{4.11}$$

To stabilise the discretised version solution of equation (4.11), the von Neumann analysis [47] method is used that require setting the value of $\Delta t/(\Delta f)^t < 1/4$.

The size of the grid is set to $\Delta f = 1$ then $\Delta t \leq 1/4$. Therefore, the value Δt is set to 1/4 for stability of equation (4.11).

4.1.1 Proposed Algorithm

The pseudo code for the proposed framework can be summarised as:

Algorithm 4.1 Proposed algorithm

Require: $f > 0$;
Initialise: $f^0 = 0$;
for $N = 1 : 1 : Iteration$ **do**
  $f^{0,0} > f^{N-1}$;
  for $k = 1 : 1 : K$ **do**
    $f^{k+1,0} = MLEM(f^{k+1,0})$;
    $f_{CD}^{k+1,0} = CD(f^{k+1,0})$;
  end for
  //Calculate the gradient coefficient
  $c(Im(f)) = \frac{\exp(i\theta)}{1+(\frac{Im(f)}{k\exp(i\theta)})^2}$
  while stop criteria is not met **do**
    // Calculate: The Proposed Model;
    for $l = 1, 2, ..., L$;(using Euler-Lagrange minimisation) **do**
      $f_j^{\hat{t+1}} = f_j^{\hat{t}} + \Delta t[\frac{(g_i - f_i)}{\sigma_i^2} + \lambda(div(c(Im(f_j^{\hat{t}}))\nabla f_j^{\hat{t}}))]$
      // update the gradient coefficient;
      $c(Im(f)) = \frac{\exp(i\theta)}{1+(\frac{Im(f)}{k\exp(i\theta)})^2}$
    end for
  end while
end for

4.2 Method and Model for Hybrid Regularization

In this section, the problems faced in the existing methods, the mathematical model and the algorithm for the proposed model is explained. The main problem of Lowdose CT image reconstruction considered in this work is an ill-posed problem either due to the scarcity of X-Ray projections data or due to the presence of noise and other inconsistencies in the acquired sinogram CT data [37]. Therefore, the image estimation that directly optimizes the Maximum Likelihood (ML) criterion can be very noisy and unstable. So researchers reformulate this problem with the maximum a posteriori (MAP) estimation by applying a prior term to penalize the solution. The prior term enables us to incorporate available information or

expected properties of the image to be reconstructed. Perona and Malik (P-M) have introduced the first partial differential equation (PDE) based on nonlinear anisotropic diffusion (AD) filter [28]. Although this method can retain the edges to some amount, it can't retain the edge details effectively for noisy images. It also causes the blocking staircase effect in the final outcome. In addition to that, it leads to smoothening out only the strong magnitude edges that affect over smoothing and lost fine edges. Therefore, to preserve the minor information as well as to produce the quality images, more robust regularization is needed. Here, in this work, a new hybrid prior is introduced as a regularization term in CT image reconstruction to reduce the limitations of the existing methods. The hybrid regularization prior is a combination of complex diffusion (CD) [31] prior and Shock prior [50]. The CD prior consists of two terms real part and an imaginary part which behaves as a real diffusion process and a second order derivative of the real part, respectively. In CD the imaginary part is used as the stopping criteria which helps to remove the noise and overcome the staircase effect of CT images. Imaginary part also plays an important role in better edge detecting. But it fails to retain the fine basic structures in the final outcome image. So,the Shock prior is used for enhancing the deblurring image by retaining the fine structures of the image. The free Schrdinger equation is combined with a diffusion equation of a complex domain by Gilboa to form a nonlinear complex diffusion with a complex value diffusion coefficient. The block diagram for the proposed model is shown in Figure 4.2

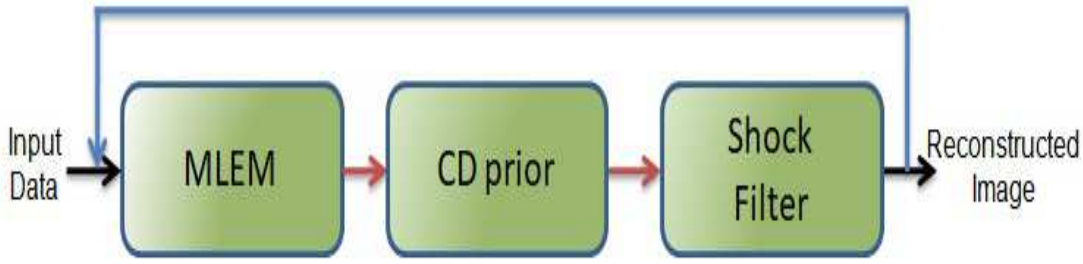

Figure 4.2: Block Diagram of Proposed Model

Here, we incorporate nonlinear complex diffusion (CD) filter and Shock filter as a regularization term with SIR method for low dose image reconstruction. The reconstructed image can be achieved by minimizing the cost function. In variational

framework [24, 47] the minimization problem can be read as:

$$f^* = \arg\min_{f \geq 0} E(f) \tag{4.12}$$

where f^* is the estimated solution i.e., the reconstructed image obtained by minimizing the energy functional $E(f)$, with constraints that all values of f must be positive. To solve the optimization problem of equation 4.12, could be equivalently written as:

$$E(f) = E_1(f) + \lambda E_2(f) \tag{4.13}$$

In equation 4.13, $E_1(f)$ is called as a data fidelity term that models the statistic of measured projection data whereas the second term represents the regularisation or smoothing term which is used as a priori knowledge of the image to be reconstructed. The balancing parameter is used to control the trade-off between data fidelity and regularisation.

In the noisy environment, the normal (Gaussian) probability distribution function (PDF) of the measured projection data is given by:

$$P(g|f) = \prod_{i=1}^{M} P(g_i|f_i) = \prod_{i=1}^{M} \frac{1}{\sqrt{2\pi\sigma_i^2}} \exp(-\frac{(g_i - f_i)^2}{2\sigma_{y_i}^2}) \tag{4.14}$$

$f = (f_1, f_2, , f_N)^T$ represents the true image vector to reconstruct the image, T represents the transpose operator, N is the number of voxels, $g = (g_1, g_2, ..., g_M)^T$ is the measured data, M is the total number of sampling points in the projection data. $P(g|f)$ is the probability of the detected measurement vector g with image intensity f. By taking the negative log-likelihood of the approximated data after elimination of constant and irrelevant terms results in the function is given by:

$$E_1(f) = \ln P(g|f) = \Sigma_{i=1}^{M} \{\frac{(g_i - f_i)^2}{2\sigma_{y_i}^2}\} \tag{4.15}$$

In the MAP estimation, the regularisation is used as *priori* information aiming to provide the solution of the ill-posedness problem in the reconstruction algorithm images [44]. Since the ideal requirement for any regularisation term is to achieve

the optimal reconstructed image with preserved features while keeping low radiations, a robust regularisation method is required. Therefore, we choose a nonlinear CD regularisation term due to the following reason:

a) It preserves the edges and minor information in the noisy projection data

b) It provides the reconstructed image in an acceptable computational time.

Thus, the regularisation function can be written as:

$$E_2(f) = \arg\min(div(c(Im(f))\nabla f) + (-sign(f_{xx})|f_x|)) \tag{4.16}$$

where $Im(.)$ is the imaginary value and the diffusion coefficient $c(Im(f))$ is defined as:

$$c(Im(f)) = \frac{\exp(i\theta)}{1 + (\frac{Im(f)}{k\exp(i\theta)})^2} \tag{4.17}$$

where k is defined as threshold parameter. The value of phase angle θ must be less than one i.e., $(\theta << 1)$. The results of the proposed framework can be acquired by substituting equations (4.15) and (4.16) into equation (4.13), to get the modified energy function written as:

$$\begin{aligned} E(f) = \arg\min_{f\geq 0} E(f) = \Sigma_{i=1}^{M}\{\frac{(g_i - f_i)^2}{2\sigma_{y_i}^2}\} \\ + \lambda\int_{\Omega}(div(c(Im(f))\nabla f))d\Omega + (-sign(f_{xx})|f_x|) \end{aligned} \tag{4.18}$$

The functional $E(f)$ is defined on the set of $f\epsilon BV(\Omega)$ such that $\log f\epsilon L^1(\Omega)$ and f must be positive everywhere.

$$\begin{aligned} f^* = \Sigma_{i=1}^{M}\{\frac{(g_i - f_i)^2}{2\sigma_{y_i}^2}\} + \lambda(div(c(Im(f))\nabla f) + (-sign(f_{xx})|f_x|)), \\ with\ \frac{\partial f}{\partial \vec{n}} = 0\ on\ \partial\Omega \end{aligned} \tag{4.19}$$

$$f^* = \frac{(g_i - f_i)}{\sigma_i^2} + \lambda(div(c(Im(f))\nabla f) + (-sign(f_{xx})|f_x|)),\ with\ \frac{\partial f}{\partial \vec{n}} = 0\ on\ \partial\Omega \tag{4.20}$$

In equation (4.20), the consideration of Euler-Lagrange minimization technique combined with the gradient descent approach provides the optimum solution.

For digital implementations, the equation (4.20) can be discretised using finite differences schemes [47]. After discretisation, the proposed model reads as:

$$\frac{f_j^{\hat{t+1}} - f_j^{\hat{t}}}{\Delta t} = \frac{(g_i - f_i)}{\sigma_i^2} + \lambda(div(c(Im(f_j^{\hat{t}}))\nabla f_j^{\hat{t}}) + (-sign(f_{xx})|f_x|)), \quad with \ \frac{\partial f}{\partial \vec{n}} = 0 \ on \ \partial\Omega \tag{4.21}$$

$$f_j^{\hat{t+1}} = f_j^{\hat{t}} + \Delta t[\frac{(g_i - f_i)}{\sigma_i^2} + \lambda(div(c(Im(f_j^{\hat{t}}))\nabla f_j^{\hat{t}}) + (-sign(f_{xx})|f_x|))] \tag{4.22}$$

To stabilise the discretised version solution of equation (4.22), the von Neumann analysis [47] method is used that require setting the value of $\Delta t/(\Delta f)^t < 1/4$. The size of the grid is set to $\Delta f = 1$ then $\Delta t \leq 1/4$. Therefore, the value Δt is set to $1/4$ for stability of equation (4.22).

4.2.1 Proposed algorithms

The pseudo code for the proposed framework can be summarised as:

Algorithm 4.2 Proposed algorithm

Require: $f > 0$;
Initialise: $f^0 = 0$;
for $N = 1 : 1 : Iteration$ **do**
  $f^{0,0} > f^{N-1}$;
  for $k = 1 : 1 : K$ **do**
    $f^{k+1,0} = MLEM(f^{k+1,0})$;
    $f_{CD}^{k+1,0} = CD(f^{k+1,0})$;
    $f_{Shock}^{k+1,0} = Shock(f_{CD}^{k+1,0})$;
  end for
  //Calculate the gradient coefficient
  $c(Im(f)) = \frac{\exp(i\theta)}{1+(\frac{Im(f)}{k\exp(i\theta)})^2}$
  while stop criteria is not met **do**
    // Calculate: The Proposed Model;
    for $l = 1, 2, ..., L$;(using Euler-Lagrange minimisation) **do**

$f_j^{t\hat{+}1} = f_j^{\hat{t}} + \Delta t[\frac{(g_i - f_i)}{\sigma_i^2} + \lambda(div(c(Im(f_j^{\hat{t}}))\nabla f_j^{\hat{t}}) + (-sign(f_{xx})|f_x|))]$

// update the gradient coefficient;

$c(Im(f)) = \frac{\exp(i\theta)}{1+(\frac{Im(f)}{k\exp(i\theta)})^2}$

end for

end while

end for

The results of the proposed methods are discussed in the next chapter.

Chapter 5

Experimental Results

In this chapter, the results of the proposed methods compared with the existing methods, on the basis of both qualitative as well as quantitative measures has been presented. In Section 5.1 the results for first proposed method are discussed and In Section 5.2 the results for the second proposed method have been discussed.

5.1 Experimental Results for MLEM+CD

In this section, the comparison has been made between the reconstruction algorithm of the proposed MLEM+CD approach and existing standard approaches available in the literature namely; MLEM [14], MLEM+AD [34], MLEM+TV [37], MLEM +NLM [24] and MLEM+AwTV [44] for X-ray CT with low dose imaging. We have compared and analyzed the performance evaluation of the proposed $MLEM + CD$ approach with other state-of-the-art approaches on the set of four test phantoms using visual inspection and quantitative measures like like peak signal-to-noise ratio (PSNR), the root mean square error (RMSE), mean structure similarity index map (MSSIM) and the correlation parameter (CP) All the results were performed for 1,000 number of iterations. In the implementation of $MLEM + AD$ the value of kappa was set between 1/100 to 1/300, number of iterations of AD were 310, $delta\_t$ was 1/7. In $MLEM + TV$ the value of theta was kept as 1216. In $MLEM + NLM$ the degree of filtering was set as 12, radio of the window from 15. The number of iterations was 100, the value of lambda is set to 0.1, value of alpha is set to 5, and these parameters were also set for the implementation of $MLEM + AwTV$. The threshold value k was set to be either one or two.The proposed and the compared methods have been implemented in MATLAB v2015b on a PC with Intel(R) No. of Core/No. of threads (4/8) i7 CPU 630 @ 3.6 GHz, 8.00 GB RAM, and Microsoft Windows (64-bit) OS.

5.1.1 Evaluation based on visualisation

Figures 5.1- 5.4 shows the output images reconstructed using the proposed model and other models from the four test phantoms. The experimental results show that the proposed model ($MLEM + CD$) is visually better than all the compared approaches in all the four test cases. It is analyzed that in the comparison models results in some there is noise, in some edges are not properly defined and some are not clear. But the proposed model results are able to preserve the edges and remove the noise and better than all other approaches.

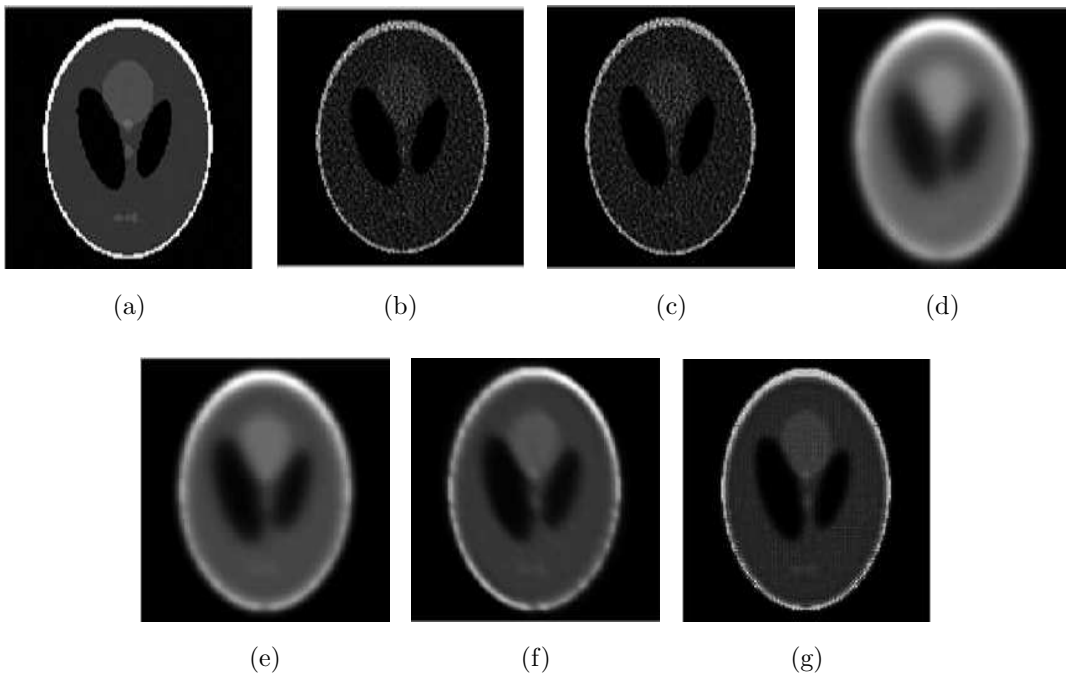

(a) (b) (c) (d)

(e) (f) (g)

Figure 5.1: The reconstructed results of Shepp−Logan head Phantom using different methods, (a) original phantom, (b) MLEM (c) MLEM+AD (d) MLEM+TV (e) MLEM+NLM (f) MLEM+AwTV (g) proposed model

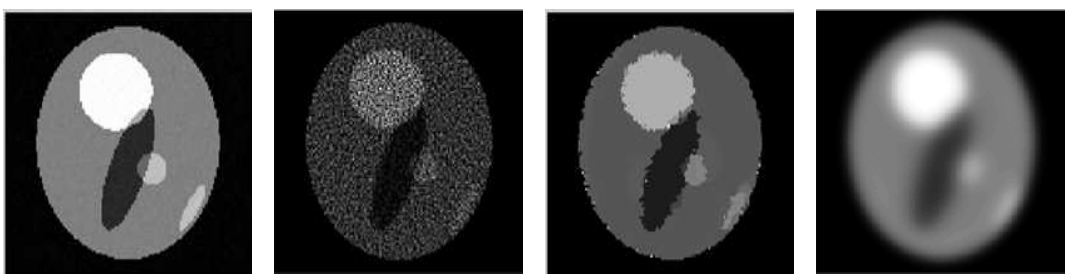

(a) (b) (c) (d)

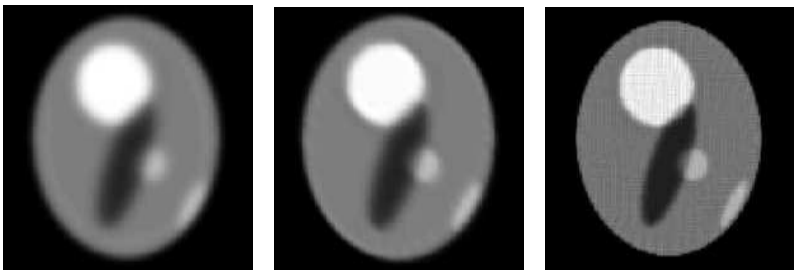

(e) (f) (g)

Figure 5.2: The reconstructed results of PET using different methods, (a) original phantom, (b) MLEM (c) MLEM+AD (d) MLEM+TV (e) MLEM+NLM (f) MLEM+AwTV (g) proposed model

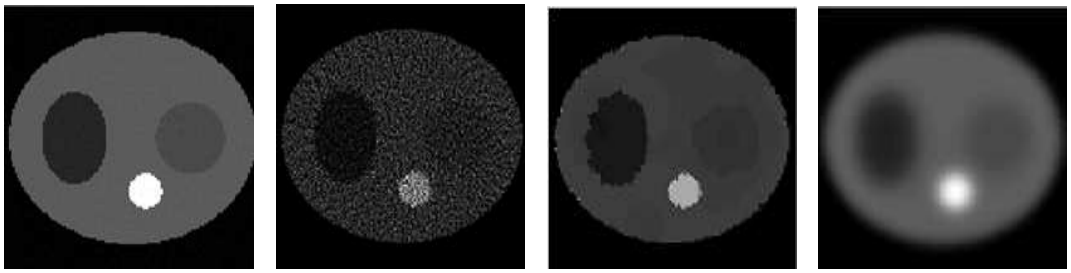

(a) (b) (c) (d)

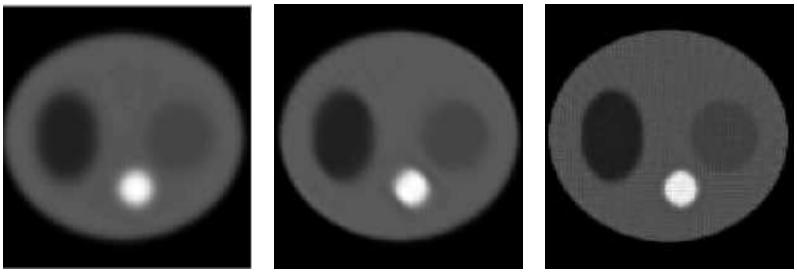

(e) (f) (g)

Figure 5.3: The reconstructed results of SPECT using different methods, (a) original phantom, (b) MLEM (c) MLEM+AD (d) MLEM+TV (e) MLEM+NLM (f) MLEM+AwTV (g) proposed model

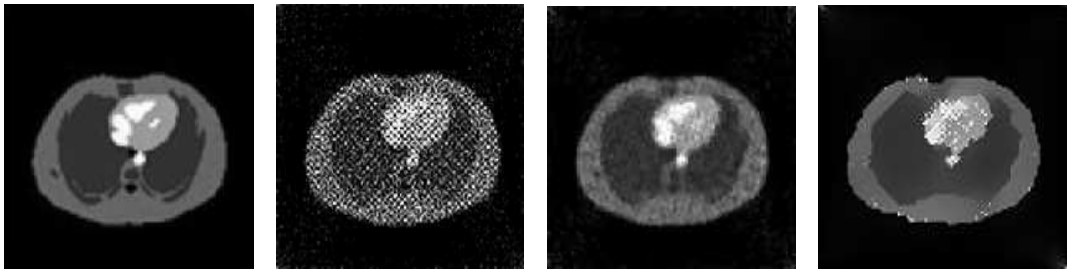

(a) (b) (c) (d)

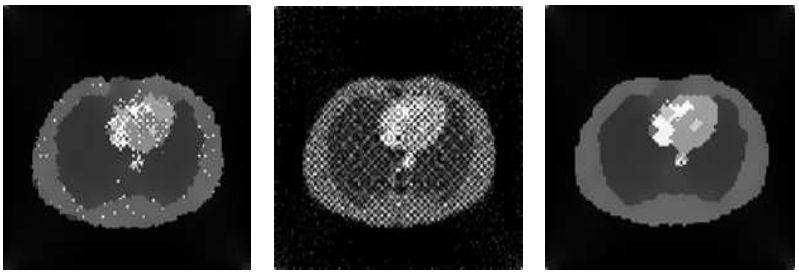

(e) (f) (g)

Figure 5.4: The reconstructed results of real thorax phantom using different methods, (a) original phantom, (b) MLEM (c) MLEM+AD (d) MLEM+TV (e) MLEM+NLM (f) MLEM+AwTV (g) proposed model

5.1.2 Evaluation based on plots

Figures 5.5- 5.8 shows the various results for the quantitative measures like peak signal-to-noise ratio (PSNR), the root mean square error (RMSE), mean structure similarity index map (MSSIM) and the correlation parameter (CP) of the proposed and compared models. All the Figures 5.5a, 5.6a, 5.7a and 5.8a shows the comparison of the proposed model and other models on the basis of PSNR value and number of iterations. From all of them, it is clearly observed that proposed model has better performance with higher PSNR value as compared to the other models. Higher value of PSNR indicates that the quality of the reconstructed image is improved. Furthermore, it is observed for all the test cases that the proposed method is producing better reconstructed image in 100-150 iterations whereas other methods are taking much higher number of iterations.

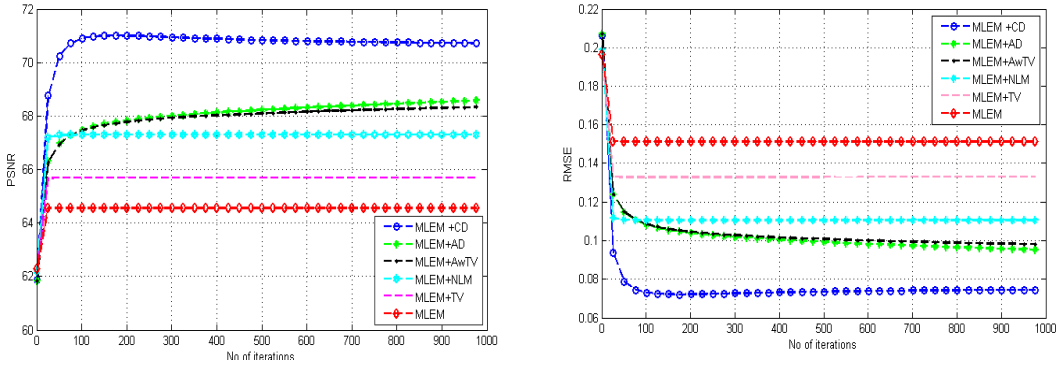

(a) (b)

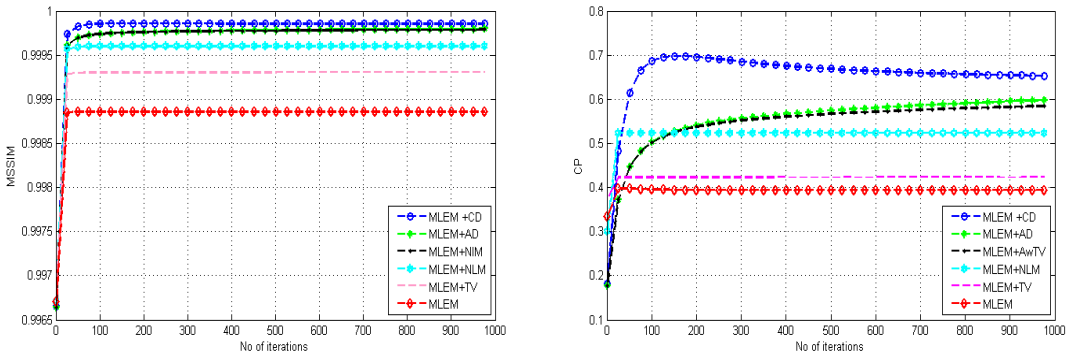

(c) (d)

Figure 5.5: The reconstructed results of Shepp−Logan head phantom using different methods, (a) original phantom, (b) MLEM (c) MLEM+AD (d) MLEM+TV (e) MLEM+NLM (f) MLEM+AwTV (g) proposed model

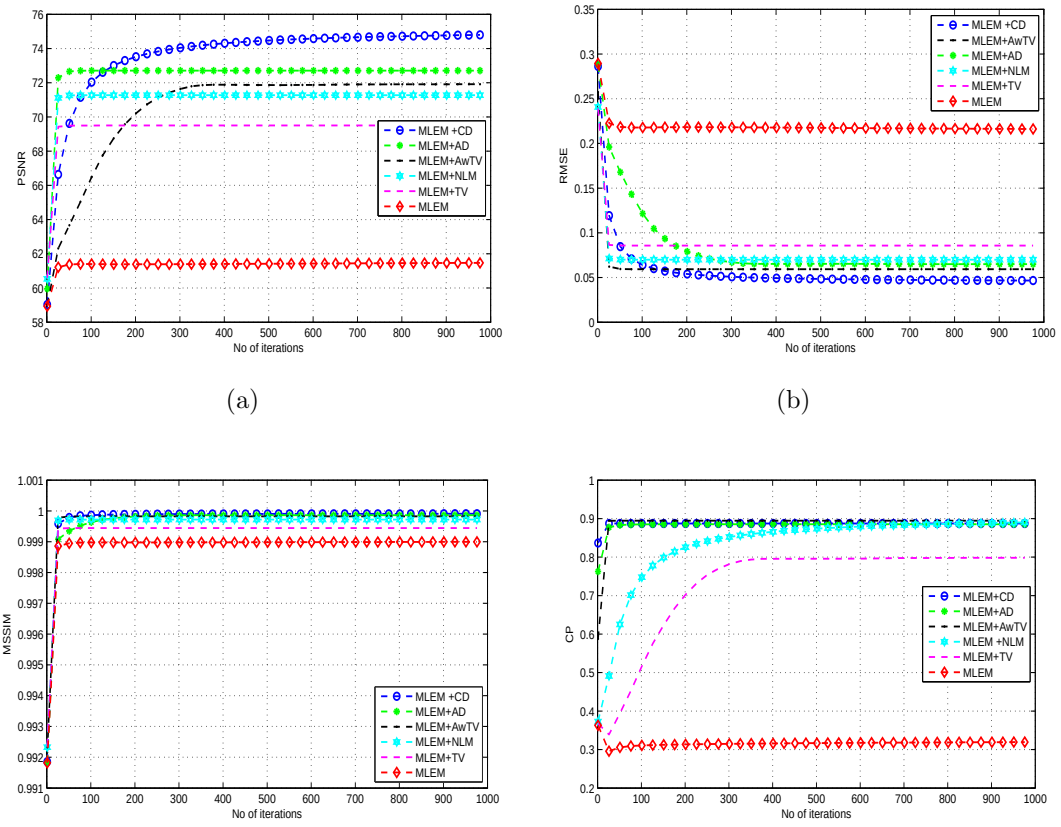

(a) (b)

(c) (d)

Figure 5.6: The reconstructed results of PET using different methods, (a) original phantom, (b) MLEM (c) MLEM+AD (d) MLEM+TV (e) MLEM+NLM (f) MLEM+AwTV (g) proposed model

Figures 5.5b, 5.6b, 5.7b and 5.8b are plotted between RMSE value and number of

iterations. RMSE value for the proposed is smaller as compared to other values. Lesser value of RMSE means that the reconstructed images are more accurate and have less error. In Figures 5.5c, 5.6c, 5.7c and 5.8c the graph is plotted between the MSSIM and number of iterations. More the MSSIM value is higher (close to unity) indicates that contrast and other details of the images are persevered during reconstruction. It is clearly observable that MSSIM value for the proposed model in all the four cases is higher. Hence provides good contrast and detailed images.

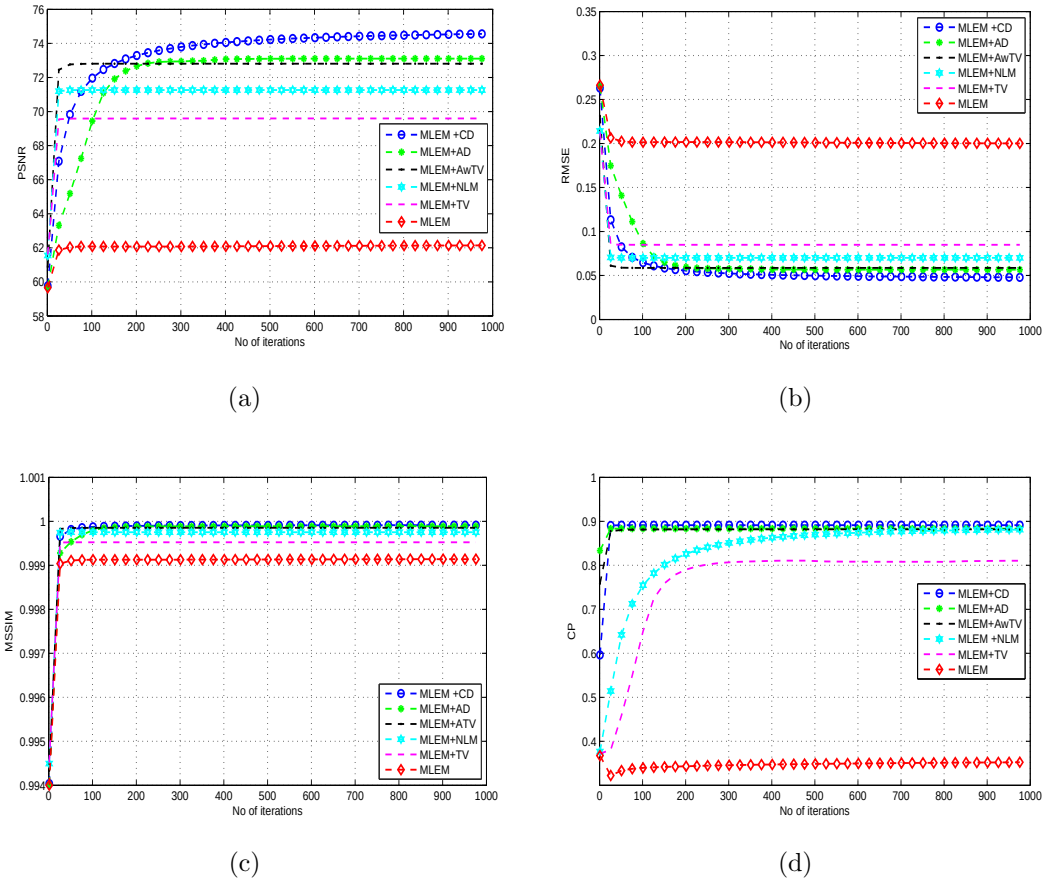

Figure 5.7: The reconstructed results of SPECT using different methods, (a) original phantom, (b) MLEM (c) MLEM+AD (d) MLEM+TV (e) MLEM+NLM (f) MLEM+AwTV (g) proposed model

Figures 5.5d, 5.6d, 5.7d and 5.8d graphs are plotted between the CP and number of iterations. For the proposed model CP value is higher as compared to the other models. This shows that the model has the capability to preserve the fine edges.

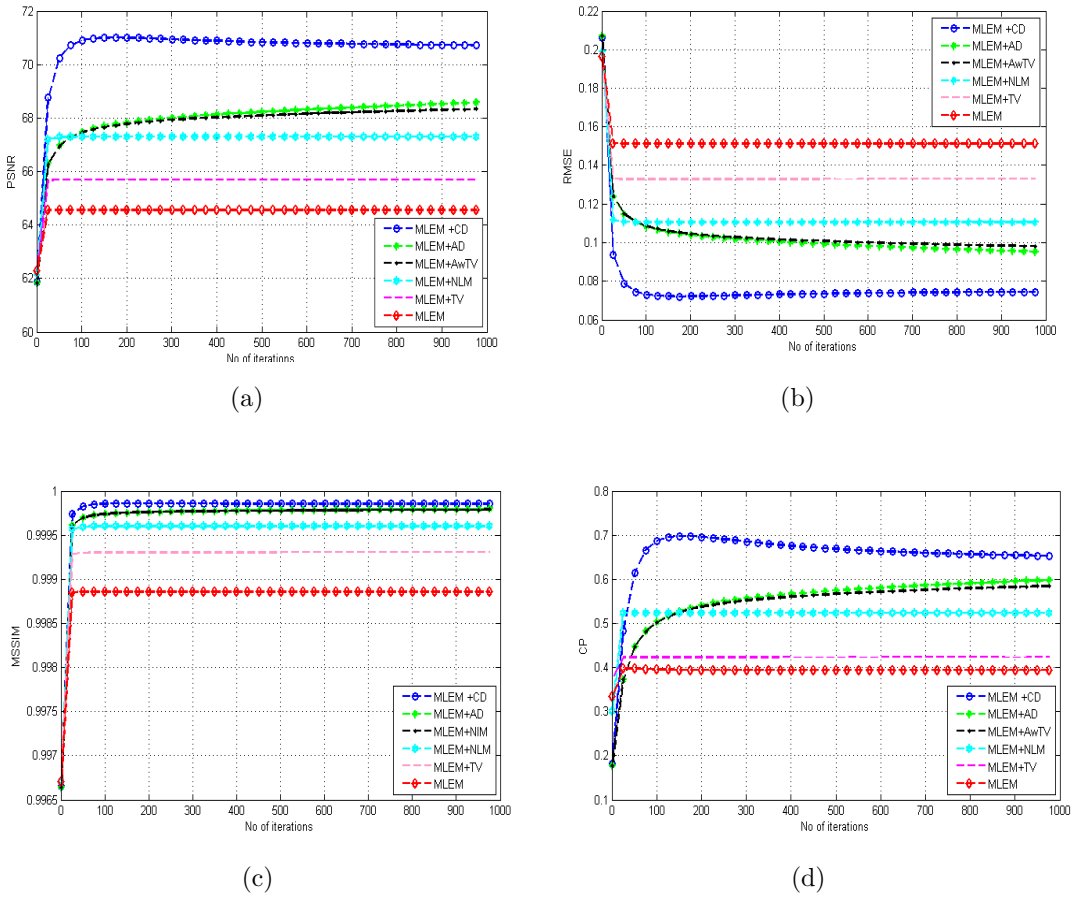

Figure 5.8: The reconstructed results of real thorax phantom using different methods, (a) original phantom, (b) MLEM (c) MLEM+AD (d) MLEM+TV (e) MLEM+NLM (f) MLEM+AwTV (g) proposed model

5.1.3 Evaluation based on quantitative measures

Tables 5.1 - 5.4 contains various quantitative parameters values like MSE, NRME, RMSE, SNR, PSNR, MSSIM, CP values. From all the tables it is clear that in all the parameters the proposed model performs better.

Table 5.1: Quantitative parameters of Shepp-Lagon phantom for test case 1

Quality Measures	MLEM	MLEM+ AD	MLEM+ TV	MLEM+ NLM	MLEM+ AwTV	MLEM+ CD
PSNR	65.5643	68.598	65.69991	67.3	68.3411	71.0055
RMSE	0.0951	0.0951	0.1328	0.1105	0.098	0.0721
MSSIM	0.9989	0.9998	0.9993	0.9996	0.9998	0.9999
CP	0.3977	0.5994	0.423	0.5239	0.5852	0.6979
SNR	0.0229	0.0091	0.0173	0.0122	0.0096	0.0052

Table 5.2: Quantitative parameters of PET phantom for test case 2

Quality Measures	MLEM	MLEM+ AD	MLEM+ TV	MLEM+ NLM	MLEM+ AwTV	MLEM+ CD
PSNR	61.4471	72.5046	69.5019	71.2689	72.7018	74.7284
RMSE	0.2167	0.0607	0.0857	0.07	0.0593	0.047
MSSIM	0.999	0.9999	0.9994	0.9997	0.9998	0.9999
CP	0.3669	0.8284	0.8848	0.8867	0.8901	0.8940
SNR	0.047	0.0037	0.0073	0.0049	0.0035	0.0022

Table 5.3: Quantitative parameters of SPECT phantom for test case 3

Quality Measures	MLEM	MLEM+ AD	MLEM+ TV	MLEM+ NLM	MLEM+ AwTV	MLEM+ CD
PSNR	62.1421	73.1093	69.5928	71.2615	72.8087	74.5672
RMSE	0.2	0.0566	0.0848	0.07	0.0586	0.0478
MSSIM	0.9991	0.9999	0.9995	0.9998	0.9999	0.9999
CP	0.3701	0.8833	0.8376	0.8794	0.8815	0.8910
SNR	0.04	0.0032	0.0072	0.0049	0.0034	0.0023

Table 5.4: Quantitative parameters of real thorax phantom for test case 4

Quality Measures	MLEM	MLEM+ AD	MLEM+ TV	MLEM+ NLM	MLEM+ AwTV	MLEM+ CD
PSNR	22.6604	27.6748	24.8376	24.9687	26.4891	27.7258
RMSE	23.3092	16.1648	13.3209	11.011	9.1829	8.9319
MSSIM	0.5786	0.8858	0.8081	0.8614	0.8858	0.8939
CP	0.5357	0.579	0.6119	0.6119	0.6373	0.8301
SNR	8.0187	11.1978	12.8786	14.5327	16.1096	16.3503

5.1.4 Evaluation based on profile graphs

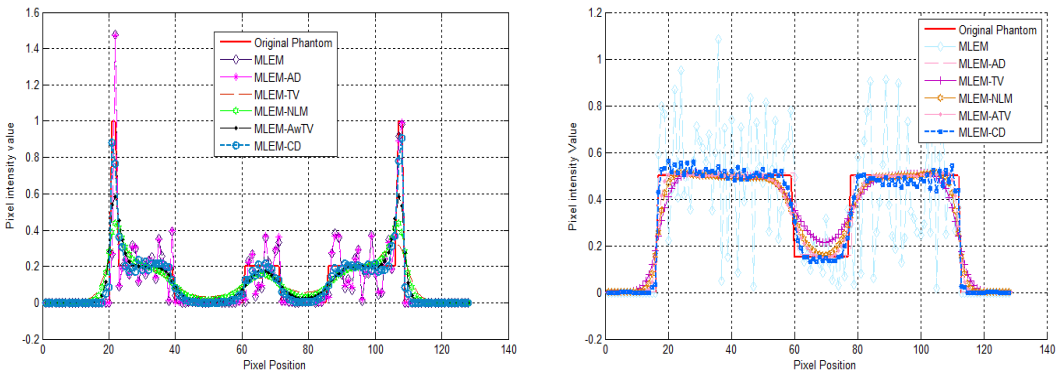

(a) (b)

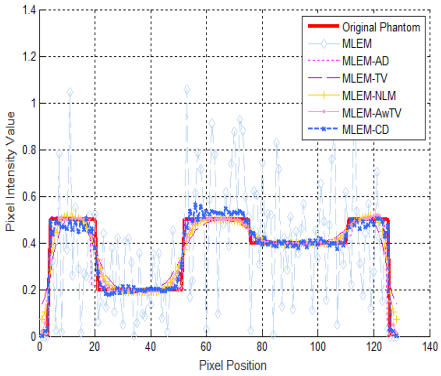

(c)

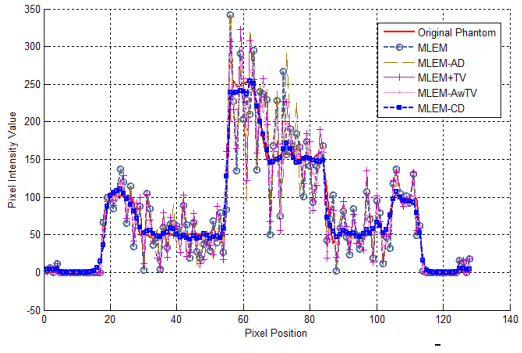

(d)

Figure 5.9: (a) Profiles along the middle row of Shepp-Logan phantom (b) Profiles along the middle row of PET phantom (c) Profiles along the middle row of SPECT phantom (d) Profiles along the middle row of original phantom

Figure 5.9 shows the profile graphs plotted between the pixel position and pixel intensity values for all the four test cases. These graphs depict the accuracy of the model. In the test cases, the experimental results show that proposed model is more accurate or close to the original image as compared to the other models.

5.2 Experimental Results for Hybrid Regularization

In this section, the comparison has been made between the proposed approach and existing standard approaches available in the literature namely; MLEM [14], MLEM+AD [34], MLEM+TV [37], MLEM +NLM [24], MLEM+AwTV [44] and MLEM+CD for X-ray CT with low dose imaging. We have compared and analyzed the performance evaluation of the proposed hybrid approach with other state-of-the-art approaches that are on the set of four test phantoms using visual inspection and quantitative measures like PSNR, the RMSE, MSSIM and the CP. To implement the other standard methods, the value of the different parameter has to be chosen optimally after rigorous experimental works. In the implementation of MLEM+AD [34] the value of kappa was set between 1/100 to 1/300, numbers of iterations of AD were between 3 to 10, *delta_t* value was kept as 1/7. In MLEM+TV [37] the value of theta was kept as between 12 to 16 degree. In MLEM+NLM [24] the degree of filtering was set as 12, the ratio of the window

size from 1 to 5. The number of iterations was 100, the value of lambda is set to 0.1, the value of alpha is set to 5, and these parameters were also set for the implementation of MLEM+AwTV [44]. The threshold value k for MLEM+CD was set between 1 to 5. For the proposed model, the parameters for complex diffusion were same whereas in case of Shock filter the iterations were kept as 500 and the mask size was set to be 9 and the value of dt as 0.1. All the results were performed for 1 - 2 number of iterations.The proposed and the compared methods have been implemented in MATLAB v2015b on a PC with Intel(R) No. of Core/No. of threads (4/8) i7 CPU 630 @ 3.6 GHz, 8.00 GB RAM, and Microsoft Windows (64-bit) OS.

5.2.1 Evaluation based on visualisation

Figures 5.10 – 5.13 shows the output images reconstructed for the proposed model i.e Hybrid Regularization and all other comparison models for all the four test phantoms.

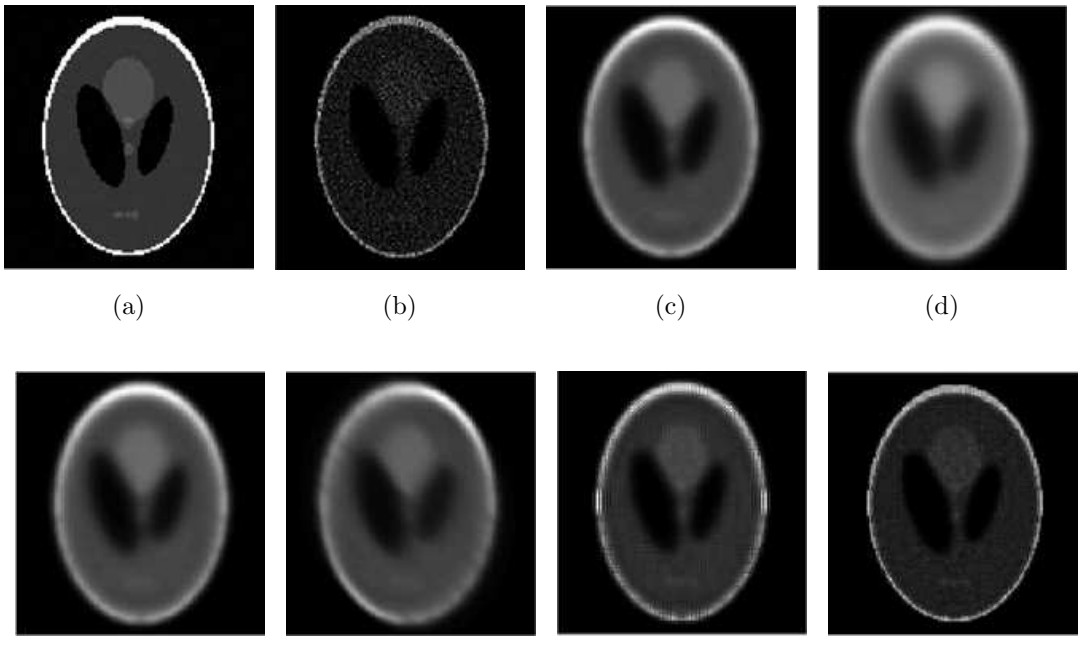

Figure 5.10: The reconstructed results of Shepp−Logan head Phantom using different methods, (a) original phantom, (b) MLEM (c) MLEM+AD (d) MLEM+TV (e) MLEM+NLM (f) MLEM+AwTV (g) MLEM+CD (h)proposed model

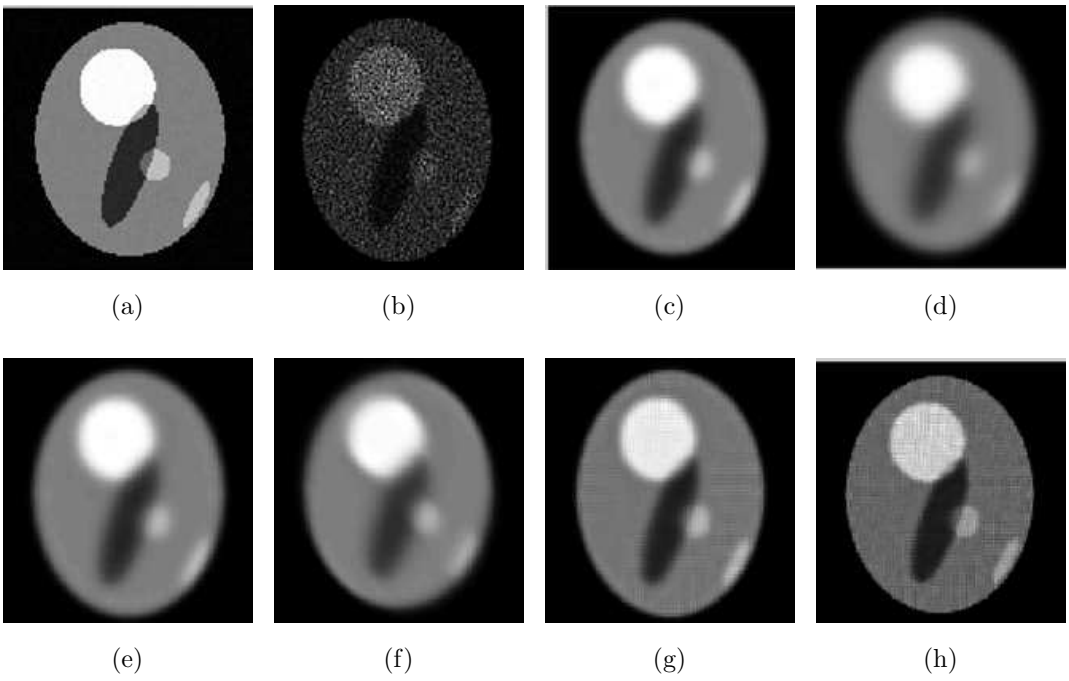

(a) (b) (c) (d)

(e) (f) (g) (h)

Figure 5.11: The reconstructed results of PET using different methods, (a) original phantom, (b) MLEM (c) MLEM+AD (d) MLEM+TV (e) MLEM+NLM (f) MLEM+AwTV (g) MLEM+CD (h) proposed model

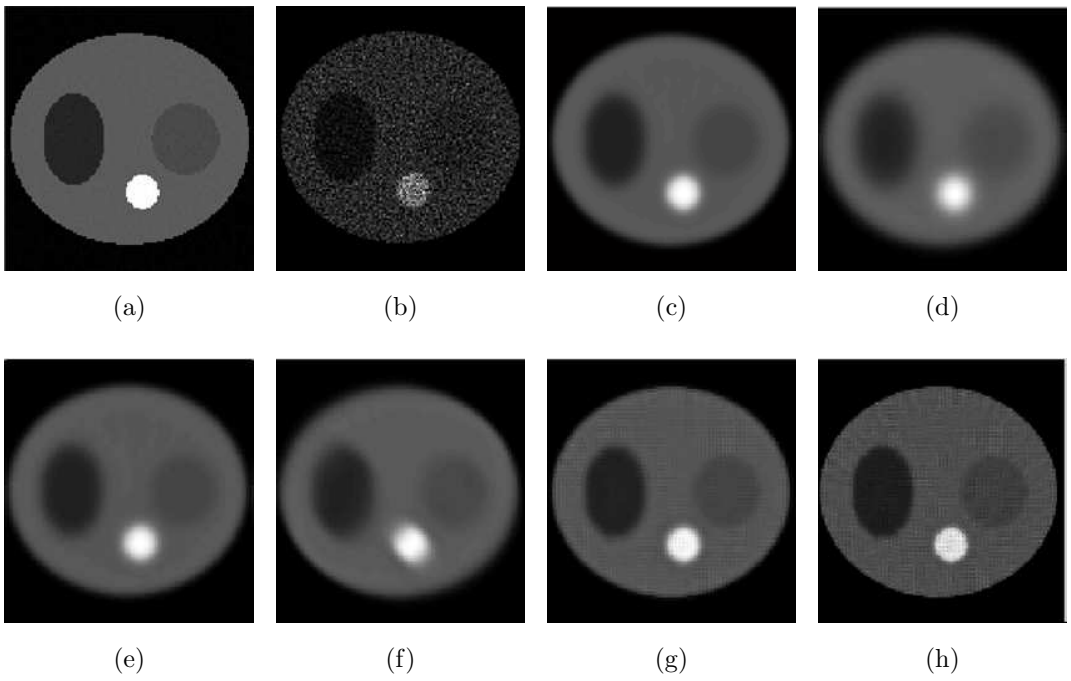

(a) (b) (c) (d)

(e) (f) (g) (h)

Figure 5.12: The reconstructed results of SPECT using different methods, (a) original phantom, (b) MLEM (c) MLEM+AD (d) MLEM+TV (e) MLEM+NLM (f) MLEM+AwTV (g) MLEM+CD (h) proposed model

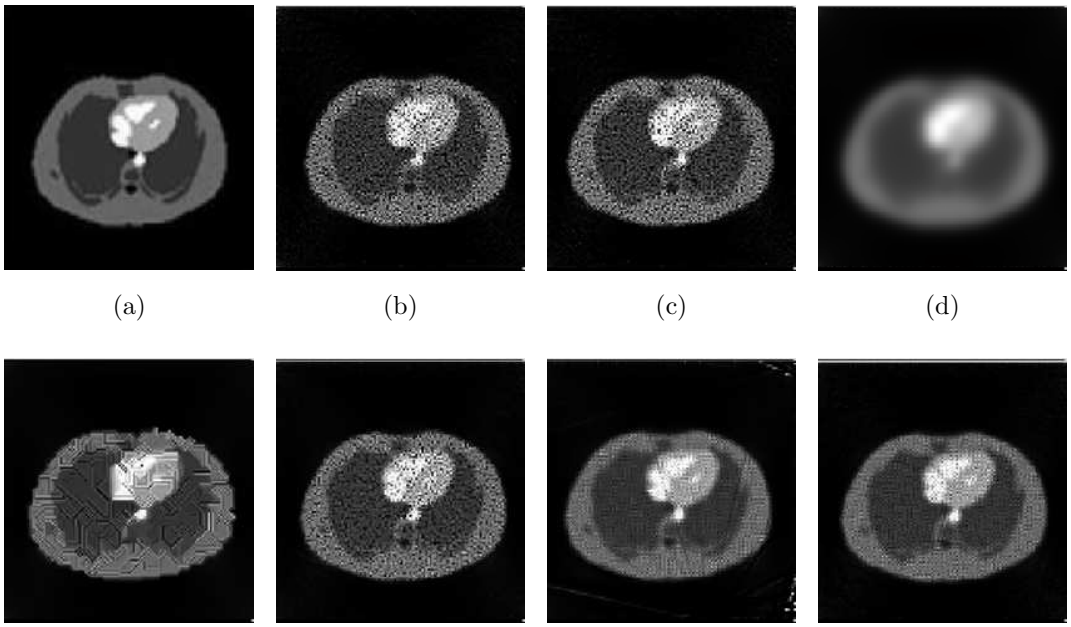

(a) (b) (c) (d)

(e) (f) (g) (h)

Figure 5.13: The reconstructed results of real thorax phantom using different methods, (a) original phantom, (b) MLEM (c) MLEM+AD (d) MLEM+TV (e) MLEM+NLM (f) MLEM+AwTV (g) MLEM+CD (h) proposed model

It is observed that the proposed model in all the four phantoms has shown better results as compared to the other models in the experimental results. From the results it is analyzed found that in the comparison models results in some there is noise, in some edges are not properly defined and some are not clear. And the proposed model results are able to preserve the edges and remove the noise.

5.2.2 Evaluation based on plots

Figures 5.14-5.17 shows the various results for the quantitative measures like peak signal-to-noise ratio (PSNR), the root mean square error (RMSE), mean structure similarity index map (MSSIM) and the correlation parameter (CP) of the proposed and compared models. All the Figures 5.14a, 5.15a, 5.16a and 5.17a shows the comparison of the proposed model and other models on the basis of PSNR value and number of iterations. From all of them, it is clearly observed that proposed model has better performance with higher PSNR value as compared to the other models. Higher value of PSNR indicates that the quality of the reconstructed image is improved.

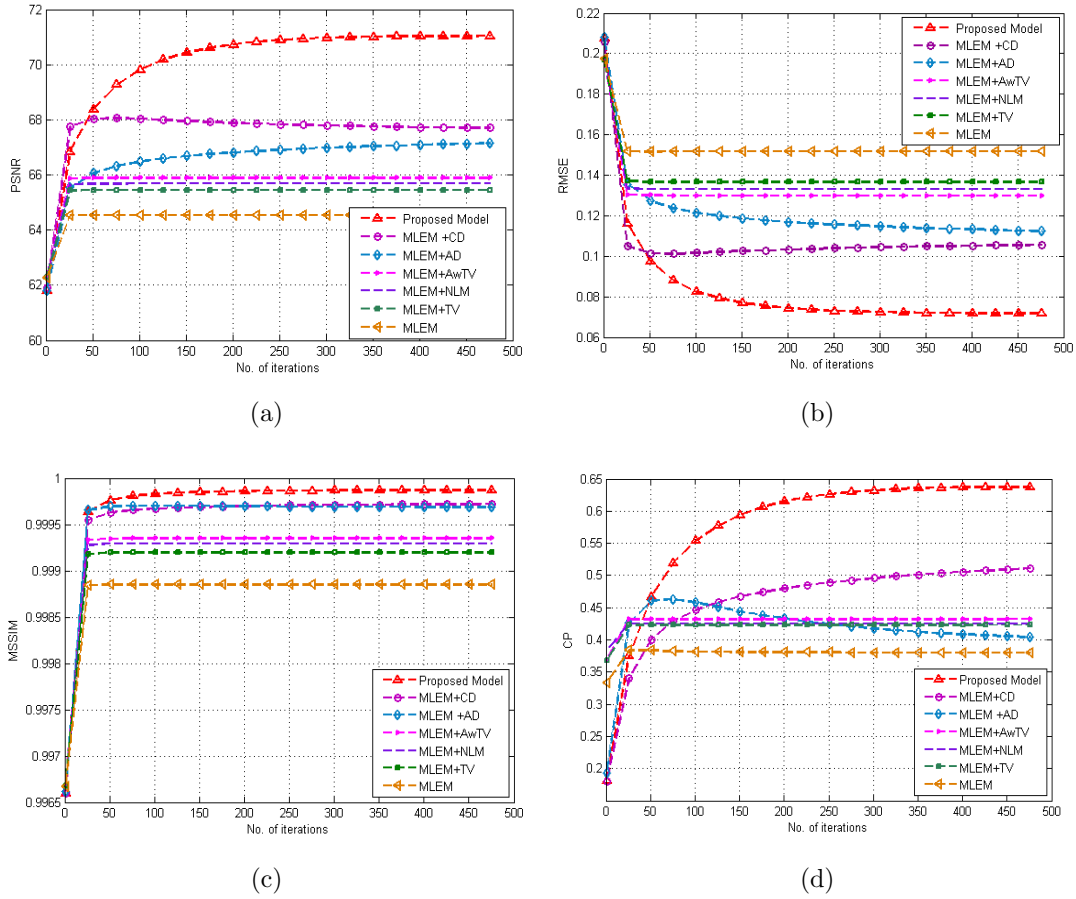

Figure 5.14: Convergence plot of iterations vs. error metrics, (a) PSNR (b) RMSE (c) MSSIM (d) CP for Shepp-Lagon phantom

Figures 5.14b, 5.15b, 5.16b and 5.17b are plotted between RMSE value and number of iterations. RMSE value for the proposed is smaller as compared to other values. Lesser value of RMSE means that the reconstructed images are more accurate and have less error.

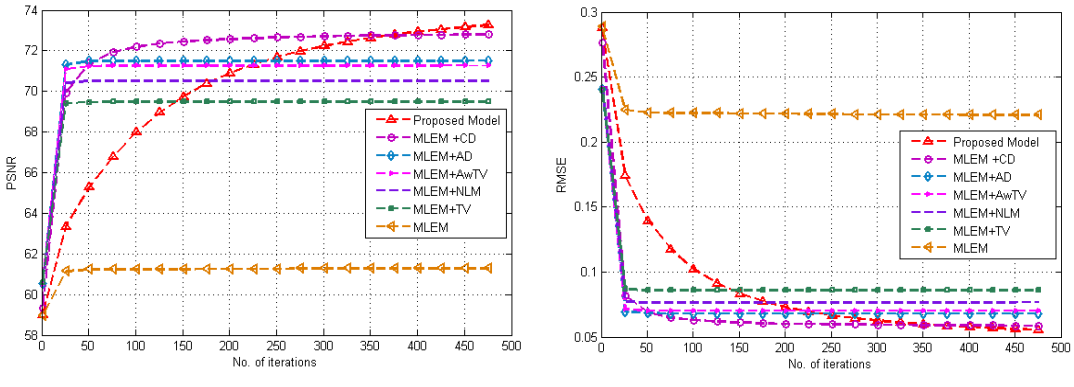

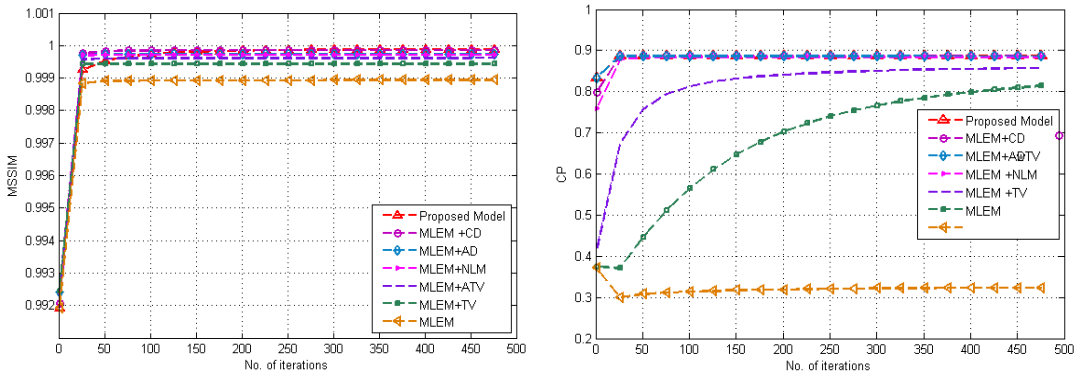

(c) (d)

Figure 5.15: Convergence plot of iterations vs. error metrics, (a) PSNR (b) RMSE (c) MSSIM (d) CP for PET phantom

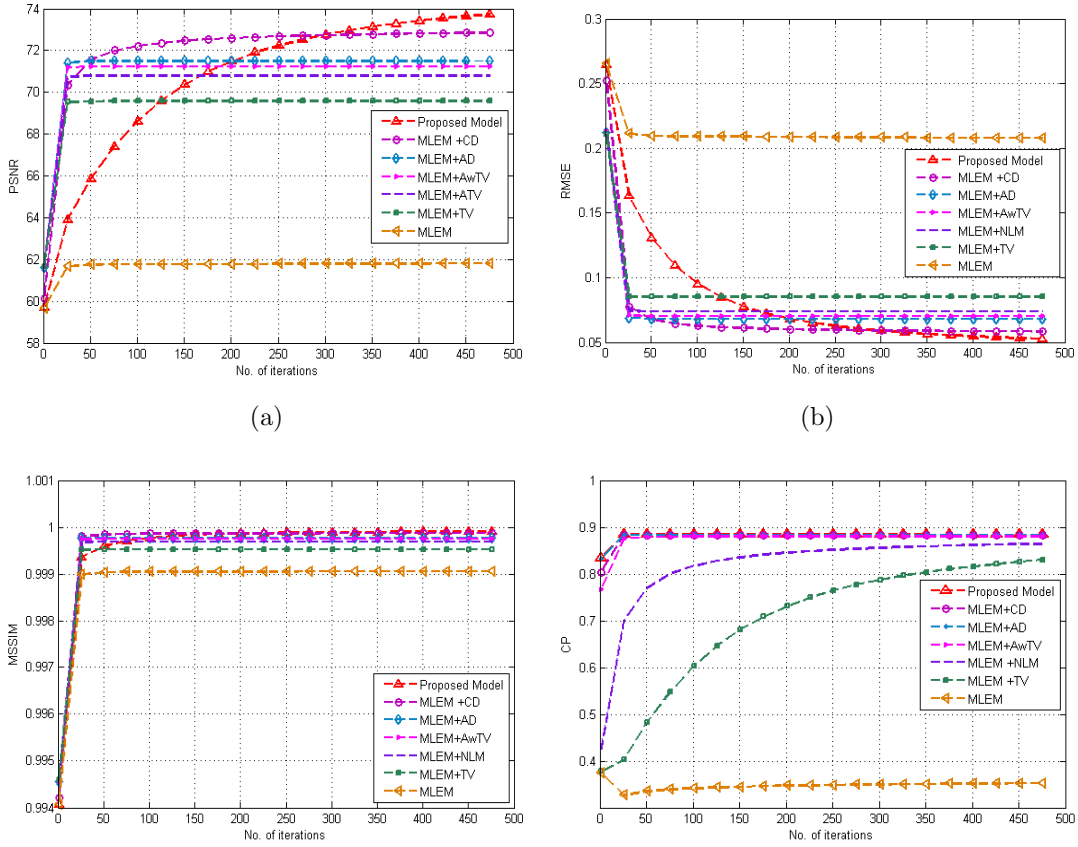

(a) (b)

(c) (d)

Figure 5.16: Convergence plot of iterations vs. error metrics, (a) PSNR (b) RMSE (c) MSSIM (d) CP for SPECT phantom

In Figures 5.14c, 5.15c, 5.16c and 5.17c the graph is plotted between the MSSIM and number of iterations. More the MSSIM value is higher (close to unity) indi-

cates that contrast and other details of the images are persevered during reconstruction. It is clearly observable that MSSIM value for the proposed model in all the four cases is higher. Hence provides good contrast and detailed images.

Figures 5.14d, 5.15d, 5.16d and 5.17d graphs are plotted between the CP and number of iterations. For the proposed model CP value is higher as compared to the other models. This shows that the model has the capability to preserve the fine edges.

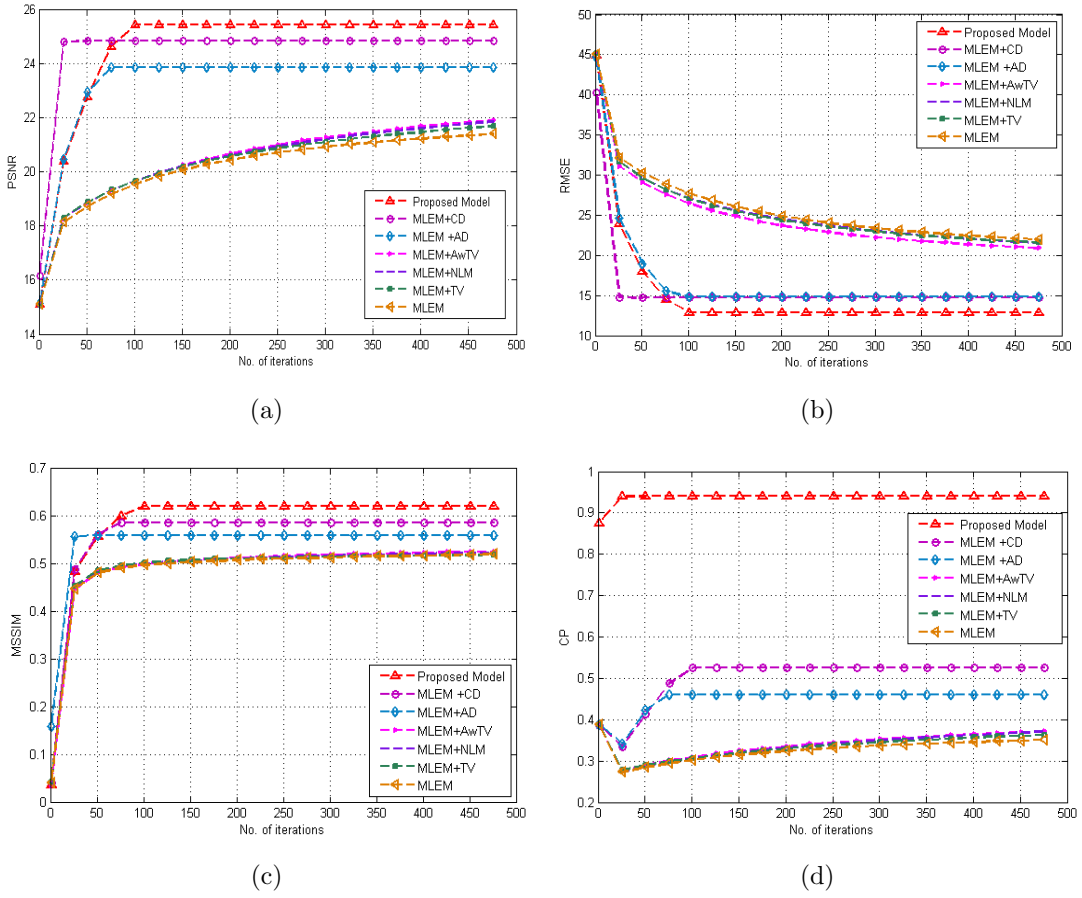

Figure 5.17: Convergence plot of iterations vs. error metrics, (a) PSNR (b) RMSE (c) MSSIM (d) CP for real thorax phantom

5.2.3 Evaluation based on quantitative measures

Tables 5.5 – 5.8 contains various quantitative parameters values like RMSE, PSNR, MSSIM, CP values. From all the tables it is observed that the proposed model performs better for all the parameters.

Table 5.5: Quantitative Parameters of Shepp Lagon head Phantom for Test case 1

Quality Measures	MLEM	MLEM+ AD	MLEM+ TV	MLEM+ NLM	MLEM+ AwTV	MLEM+ CD	Proposed Model
PSNR	64.5474	67.1624	65.4517	65.6855	65.8905	68.0634	71.038
RMSE	0.1517	0.1122	0.1367	0.133	0.1299	0.1012	0.0718
MSSIM	0.9989	0.9997	0.9992	0.9993	0.9993	0.9997	0.9999
CP	0.384	0.4636	0.4231	0.4248	0.4319	0.5123	0.6375

Table 5.6: Quantitative Parameters of PET Phantom for Test case 2

Quality Measures	MLEM	MLEM+ AD	MLEM+ TV	MLEM+ NLM	MLEM+ AwTV	MLEM+ CD	Proposed Model
PSNR	61.2857	71.5038	69.4806	70.5182	71.2568	72.8132	73.3529
RMSE	0.2208	0.0681	0.0859	0.0763	0.07	0.0586	0.055
MSSIM	0.9989	0.9997	0.9994	0.9996	0.9997	0.9999	0.9999
CP	0.3709	0.8874	0.8836	0.8868	0.8868	0.858	0.8181

Table 5.7: Quantitative Parameters of SPECT Phantom for Test case 3

Quality Measures	MLEM	MLEM+ AD	MLEM+ TV	MLEM+ NLM	MLEM+ AwTV	MLEM+ CD	Proposed Model
PSNR	61.8056	71.4936	69.5718	70.7937	71.244	72.8598	73.8109
RMSE	0.2079	0.0682	0.085	0.0739	0.0702	0.0582	0.0522
MSSIM	0.9991	0.9998	0.9995	0.9997	0.9998	0.9999	0.9999
CP	0.3752	0.8841	0.8797	0.8836	0.8835	0.8649	0.8332

Table 5.8: Quantitative Parameters of real thorax Phantom for Test case 4

Quality Measures	MLEM	MLEM+ AD	MLEM+ TV	MLEM+ NLM	MLEM+ AwTV	MLEM+ CD	Proposed Model
PSNR	21.2348	24.8253	21.4025	21.6163	21.6479	25.8108	26.5977
RMSE	22.2074	14.6884	21.7829	21.2532	20.7616	14.8008	12.9124
MSSIM	0.5138	0.5598	0.5207	0.5209	0.5214	0.6358	0.6546
CP	0.3813	0.9399	0.3869	0.3845	0.3926	0.5474	0.5784

5.2.4 Evaluation based on profile graphs

Figure 5.18 shows the profile graphs plotted between the pixel position and pixel intensity values for all the four test cases. These graphs depict the accuracy of the model. In the test cases, the experimental results show that proposed

model is more accurate or close to the original image as compared to the other models.

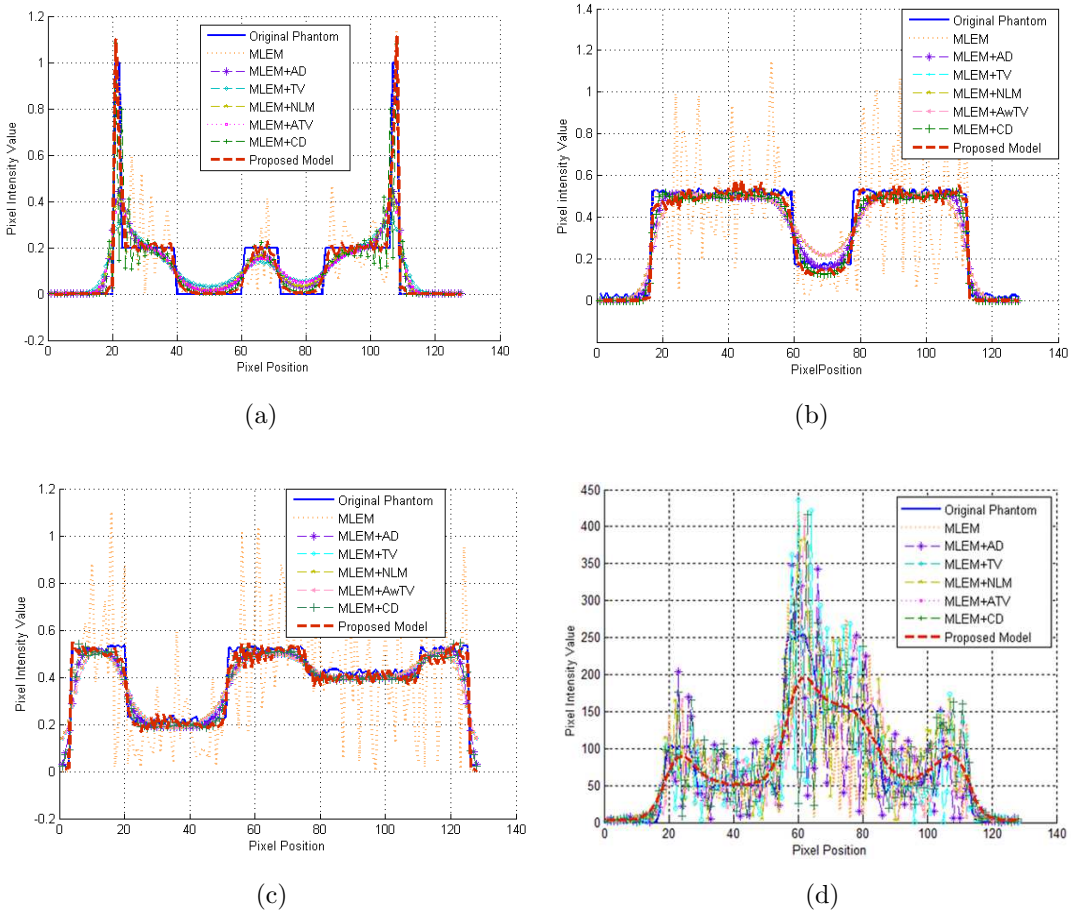

Figure 5.18: (a) Profiles along the middle row of Shepp-Logan phantom (b) Profiles along the middle row of PET phantom (c) Profiles along the middle row of SPECT phantom (d) Profiles along the middle row of original phantom

Chapter 6

Conclusion and Future Work

In this chapter, the conclusions of the thesis are stated and the scope for future research has been discussed. In this thesis, to remove the Gaussian noise as well as the ill-posedness issue for the low dose projection data, new methods were proposed. In the first proposed method Complex Diffusion filter was used as regularization term with MLEM. While in the other method a hybrid regularization prior (combination of CD and Shock) was used. The proposed methods were compared with the MLEM based iterative reconstruction method and its various variants. The comparative performance evaluation and the study of the proposed method exhibit its better capability to remove the noise and preserve the minor information.

In the future optimization of the parameters, an important strategy for the solution of an inverse problem with the minimization of the least square functional can be performed. And it can also be designed to handle the poisson noise.

References

[1] A. P. Dhawan, "Principles of image reconstruction methods," in *Principles and Advanced Methods in Medical Imaging and Image Analysis*. World Scientific, 2008.

[2] H. Zhang, "Statistical image reconstruction for low-dose x-ray computed tomography: statistical models and regularization strategies," Ph.D. dissertation, State University of New York at Stony Brook, 2016.

[3] H. Zhang, J. Ma, Y. Liu, H. Han, L. Li, J. Wang, and Z. Liang, "Nonlocal means-based regularizations for statistical ct reconstruction," in *Medical Imaging 2014: Physics of Medical Imaging*, vol. 9033. International Society for Optics and Photonics, 2014, p. 903337.

[4] C. H. McCollough, M. R. Bruesewitz, and J. M. Kofler Jr, "Ct dose reduction and dose management tools: overview of available options," *Radiographics*, vol. 26, no. 2, pp. 503–512, 2006.

[5] A. J. Devaney, "A filtered backpropagation algorithm for diffraction tomography," *Ultrasonic imaging*, vol. 4, no. 4, pp. 336–350, 1982.

[6] R. Gordon, R. Bender, and G. T. Herman, "Algebraic reconstruction techniques (art) for three-dimensional electron microscopy and x-ray photography," *Journal of theoretical Biology*, vol. 29, no. 3, pp. 471–481, 1970.

[7] P. Gilbert, "Iterative methods for the three-dimensional reconstruction of an object from projections," *Journal of theoretical biology*, vol. 36, no. 1, pp. 105–117, 1972.

[8] A. H. Andersen and A. C. Kak, "Simultaneous algebraic reconstruction technique (sart): a superior implementation of the art algorithm," *Ultrasonic imaging*, vol. 6, no. 1, pp. 81–94, 1984.

[9] D. Mishra, K. Muralidhar, and P. Munshi, "A robust mart algorithm for tomographic applications," *Numerical Heat Transfer: Part B: Fundamentals*, vol. 35, no. 4, pp. 485–506, 1999.

[10] Y. Censor, D. Gordon, and R. Gordon, "Component averaging: An efficient iterative parallel algorithm for large and sparse unstructured problems," *Parallel computing*, vol. 27, no. 6, pp. 777–808, 2001.

[11] Y. Censor, D. Gordon, and R. Gordan, "Bicav: A block-iterative parallel algorithm for sparse systems with pixel-related weighting," *IEEE Transactions on Medical Imaging*, vol. 20, no. 10, pp. 1050–1060, 2001.

[12] Y. Lin and E. Samei, "An efficient polyenergetic sart (psart) reconstruction algorithm for quantitative myocardial ct perfusion," *Medical physics*, vol. 41, no. 2, 2014.

[13] A. J. Rockmore and A. Macovski, "A maximum likelihood approach to emission image reconstruction from projections," *IEEE transactions on nuclear science*, vol. 23, no. 4, pp. 1428–1432, 1976.

[14] L. A. Shepp and Y. Vardi, "Maximum likelihood reconstruction for emission tomography," *IEEE transactions on medical imaging*, vol. 1, no. 2, pp. 113–122, 1982.

[15] H. M. Hudson and R. S. Larkin, "Accelerated image reconstruction using ordered subsets of projection data," *IEEE transactions on medical imaging*, vol. 13, no. 4, pp. 601–609, 1994.

[16] J. Browne and A. De Pierro, "A row-action alternative to the em algorithm for maximizing likelihood in emission tomography," *IEEE transactions on medical imaging*, vol. 15, no. 5, pp. 687–699, 1996.

[17] T. Hsiao and H.-M. Huang, "An accelerated ordered subsets reconstruction algorithm using an accelerating power factor for emission tomography," *Physics in Medicine & Biology*, vol. 55, no. 3, p. 599, 2010.

[18] S. Gordic, L. Desbiolles, P. Stolzmann, L. Gantner, S. Leschka, D. Husarik, and H. Alkadhi, "Advanced modelled iterative reconstruction for abdominal

ct: qualitative and quantitative evaluation," *Clinical radiology*, vol. 69, no. 12, pp. e497–e504, 2014.

[19] L. L. Geyer, U. J. Schoepf, F. G. Meinel, J. W. Nance Jr, G. Bastarrika, J. A. Leipsic, N. S. Paul, M. Rengo, A. Laghi, and C. N. De Cecco, "State of the art: iterative ct reconstruction techniques," *Radiology*, vol. 276, no. 2, pp. 339–357, 2015.

[20] S. Lee, H. Kwon, and J. Cho, "The detection of focal liver lesions using abdominal ct: a comparison of image quality between adaptive statistical iterative reconstruction v and adaptive statistical iterative reconstruction," *Academic radiology*, vol. 23, no. 12, pp. 1532–1538, 2016.

[21] J. Sun, T. Yu, J. Liu, X. Duan, D. Hu, Y. Peng *et al.*, "Image quality improvement using model-based iterative reconstruction in low dose chest ct for children with necrotizing pneumonia," *BMC medical imaging*, vol. 17, no. 1, p. 24, 2017.

[22] P. J. Green, "Bayesian reconstructions from emission tomography data using a modified em algorithm," *IEEE transactions on medical imaging*, vol. 9, no. 1, pp. 84–93, 1990.

[23] J. Wang, Z. Liang, H. Lu, and L. Xing, "Recent development of low-dose x-ray cone-beam computed tomography," *Current Medical Imaging Reviews*, vol. 6, no. 2, pp. 72–81, 2010.

[24] H. Zhang, J. Wang, J. Ma, H. Lu, and Z. Liang, "Statistical models and regularization strategies in statistical image reconstruction of low-dose x-ray ct: a survey," *arXiv preprint arXiv:1412.1732*, 2014.

[25] E. Garduño and G. T. Herman, "Superiorization of the ml-em algorithm," *IEEE Transactions on Nuclear Science*, vol. 61, no. 1, pp. 162–172, 2014.

[26] E. Levitan and G. T. Herman, "A maximum a posteriori probability expectation maximization algorithm for image reconstruction in emission tomography," *IEEE Transactions on Medical Imaging*, vol. 6, no. 3, pp. 185–192, 1987.

[27] N. Denisova, "Bayesian reconstruction in spect with entropy prior and iterative statistical regularization," *IEEE Transactions on Nuclear Science*, vol. 51, no. 1, pp. 136–141, 2004.

[28] P. Perona and J. Malik, "Scale-space and edge detection using anisotropic diffusion," *IEEE Transactions on pattern analysis and machine intelligence*, vol. 12, no. 7, pp. 629–639, 1990.

[29] L. I. Rudin, S. Osher, and E. Fatemi, "Nonlinear total variation based noise removal algorithms," *Physica D: nonlinear phenomena*, vol. 60, no. 1-4, pp. 259–268, 1992.

[30] H. Ling and A. C. Bovik, "Smoothing low-snr molecular images via anisotropic median-diffusion," *IEEE Transactions on Medical Imaging*, vol. 21, no. 4, pp. 377–384, 2002.

[31] G. Gilboa, Y. Y. Zeevi, and N. A. Sochen, "Complex difusion processes for image filtering," in *International Conference on Scale-Space Theories in Computer Vision*. Springer, 2001, pp. 299–307.

[32] A. Buades, B. Coll, and J.-M. Morel, "A non-local algorithm for image denoising," in *Computer Vision and Pattern Recognition, 2005. CVPR 2005. IEEE Computer Society Conference on*, vol. 2. IEEE, 2005, pp. 60–65.

[33] B. S. Kumar and G. Nagarajan, "Tomographic image reconstruction using sart algorithm," *International Journal of Medical Engineering and Informatics*, vol. 8, no. 3, pp. 239–248, 2016.

[34] J. Yan, "Investigation of positron emission tomography image reconstruction," *Huazhong University of Science & Technology, Wuhan, China*, 2007.

[35] H. Bhadauria and M. Dewal, "Comparative evaluation of denoising methods on brain ct images," *International Journal of Signal and Imaging Systems Engineering*, vol. 6, no. 3, pp. 182–187, 2013.

[36] Q. He and L. Huang, "Penalized maximum likelihood algorithm for positron emission tomography by using anisotropic median-diffusion," *Mathematical Problems in Engineering*, vol. 2014, 2014.

[37] L. B. Chávez-Rivera, L. Ortega-Máynez, J. Mejía, and B. Mederos, "Ml-em reconstruction model including total variation for low dose pet high resolution data," in *Nuclear Science Symposium and Medical Imaging Conference (NSS/MIC), 2015 IEEE*. IEEE, 2015, pp. 1–5.

[38] A. Boudjelal, Z. Messali, and A. Elmoataz, "A novel kernel-based regularization technique for pet image reconstruction," *Technologies*, vol. 5, no. 2, p. 37, 2017.

[39] H. Lu, T. Hsiao, X. Li, and Z. Liang, "Noise properties of low-dose ct projections and noise treatment by scale transformations," in *Nuclear Science Symposium Conference Record, 2001 IEEE*, vol. 3. IEEE, 2001, pp. 1662–1666.

[40] T. Li, X. Li, J. Wang, J. Wen, H. Lu, J. Hsieh, and Z. Liang, "Nonlinear sinogram smoothing for low-dose x-ray ct," *IEEE Transactions on Nuclear Science*, vol. 51, no. 5, pp. 2505–2513, 2004.

[41] Y. Vardi, L. Shepp, and L. Kaufman, "A statistical model for positron emission tomography," *Journal of the American statistical Association*, vol. 80, no. 389, pp. 8–20, 1985.

[42] S. Alenius and U. Ruotsalainen, "Bayesian image reconstruction for emission tomography based on median root prior," *European journal of nuclear medicine*, vol. 24, no. 3, pp. 258–265, 1997.

[43] Z. Tian, X. Jia, K. Yuan, T. Pan, and S. B. Jiang, "Low-dose ct reconstruction via edge-preserving total variation regularization," *Physics in Medicine & Biology*, vol. 56, no. 18, p. 5949, 2011.

[44] Y. Liu, J. Ma, Y. Fan, and Z. Liang, "Adaptive-weighted total variation minimization for sparse data toward low-dose x-ray computed tomography image reconstruction," *Physics in Medicine & Biology*, vol. 57, no. 23, p. 7923, 2012.

[45] Y. Wang, S. Fu, W. Li, and C. Zhang, "An adaptive nonlocal filtering for

low-dose ct in both image and projection domains," *Journal of computational design and engineering*, vol. 2, no. 2, pp. 113–118, 2015.

[46] J. Rong, W. Liu, P. Gao, Q. Liao, C. Jiao, J. Ma, and H. Lu, "Ct reconstruction from few-views with anisotropic edge-guided total variance," *Nuclear Instruments and Methods in Physics Research Section A: Accelerators, Spectrometers, Detectors and Associated Equipment*, vol. 820, pp. 54–64, 2016.

[47] S. Tiwari and R. Srivastava, "A hybrid-cascaded iterative framework for positron emission tomography and single-photon emission computed tomography image reconstruction," *Journal of Medical Imaging and Health Informatics*, vol. 6, no. 4, pp. 1001–1012, 2016.

[48] R. Srivastava, J. Gupta, and H. Parthasarthy, "A non-linear complex diffusion-based edge and structure preserving zooming technique for mri and ultrasound images," *International Journal of Biomedical Engineering and Technology*, vol. 6, no. 2, pp. 178–199, 2011.

[49] J. Amudha and R. Sudhakar, "A multi-resolution transform for deblurring of images in the presence of impulse noise for real-time images," *International Journal of Biomedical Engineering and Technology*, vol. 23, no. 2-4, pp. 97–108, 2017.

[50] S. Osher and L. I. Rudin, "Feature-oriented image enhancement using shock filters," *SIAM Journal on numerical analysis*, vol. 27, no. 4, pp. 919–940, 1990.

List of Publications

International Journal

1. Kavkirat Kaur, Shailendra Tiwari, *"Complex diffusion regularisation-based low dose CT image reconstruction"*, International Journal of Biomedical Engineering and Technology(IJBET), Inder-Science Publishers, 2018, (Scopus). [Under Press]

2. Kavkirat Kaur, Shailendra Tiwari et al., *"Computed Tomography Reconstruction using Hybrid Regularization Approach"*, IEEE Transactions on Industrial Informatics, SCI. Impact Factor 6.764. [Under Revision]

International Conference

1. Kavkirat Kaur, Shailendra Tiwari, *"Low-dose CT Image Reconstruction using Complex Diffusion Regularization"*, International Conference on Computational Intelligence: Theories, Applications and Future Directions (ICCI 2017), IIT Kanpur, India. (Indexed in Scopus, DBLP) IEEE Conference Publication Services (CPS). [Under Press]

Book Chapter

1. Kavkirat Kaur, Shailendra Tiwari, *"Dictionary Learning based Image Reconstruction Techniques for Big Medical Data"*, Deep Learning in Computer Vision: Theories and Applications, CRC Press. [Communicated]

Thesis

ORIGINALITY REPORT

18%	9%	15%	%
SIMILARITY INDEX	INTERNET SOURCES	PUBLICATIONS	STUDENT PAPERS

PRIMARY SOURCES

1	Tiwari, Shailendra, and Rajeev Srivastava. "A PDE based expectation maximization algorithm adapted to Poisson noise for medical image reconstruction", 2014 IEEE International Symposium on Signal Processing and Information Technology (ISSPIT), 2014. Publication	1%
2	"Proceedings of International Conference on Computer Vision and Image Processing", Springer Nature, 2017 Publication	1%
3	catalogimages.wiley.com Internet Source	1%
4	Hao Zhang, Hao Han, Jing Wang, Jianhua Ma, Yan Liu, William Moore, Zhengrong Liang. "Deriving adaptive MRF coefficients from previous normal-dose CT scan for low-dose image reconstruction via penalized weighted least-squares minimization", Medical Physics, 2014 Publication	1%